CBPF-NF-026/01

Nuclear photofissility in the quasi-deuteron energy region*

E. de Paiva† and O. A. P. Tavares

Centro Brasileiro de Pesquisas Físicas - CBPF/MCT
Rua Dr. Xavier Sigaud 150, 22290-180 Rio de Janeiro-RJ, Brazil

M. L. Terranova

Dipartimento di Scienze e Tecnologie Chimiche, Universitá di Roma
"Tor Vergata", and Istituto Nazionale di Fisica Nucleare – INFN,
Sezione di Roma 2, via della Ricerca Scientifica, 00133 Roma, Italy

A two hundred experimental photofissility data obtained in the quasi-deuteron region ($\sim 30 - 140$ MeV) of photonuclear absorption covering the target nuclei ^{27}Al, ^{nat}Ti, ^{51}V, ^{154}Sm, ^{174}Yb, ^{nat}Hf, ^{181}Ta, ^{nat}W, ^{nat}Re, ^{nat}Os, ^{nat}Pt, ^{197}Au, ^{nat}Tl, ^{208}Pb, ^{nat}Pb and ^{209}Bi have been analysed in the framework of the current, two-step model for intermediate-energy photofission reactions. The incoming photon is assumed to be absorbed by a neutron-proton pair (Levinger's quasi-deuteron model), followed by a mechanism of evaporation-fission competition for the excited residual nuclei. The experimental features of photofissility have been reproduced successfully by the model.

PACS number(s): 25.20.-x, 25.85.-w, 25.85.Jg

*Dedicated to the memory of Prof. Dr. Gurami Ya. Kezerashvili.

†Permanent address: Instituto de Radioproteção e Dosimetria-IRD/CNEN, Av. Salvador Allende s/n, 22780-160 Rio de Janeiro-RJ, and Sociedade Educacional São Paulo Apóstolo-UniverCidade, Rua Padre Ventura 184, 22710–260 Rio de Janeiro-RJ, Brazil.

1 Introduction

Photofission reaction studies have received much attention from researchers soon after the development of new techniques to produce high-quality monochromatic (or quasi-monochromatic) photon beams of energies greater than $\sim$ 20 MeV [1]. In particular, a considerable number of photofission cross section and fissility data for pre-actinide, intermediate-mass and less-massive nuclei ranging from ^{27}Al up to ^{209}Bi has been obtained during the last twenty years or so at incident photon energies in the quasi-deuteron region ($\sim 30 - 140$ MeV) of photonuclear absorption [2-13]. Also available are a number of measured photofission cross section values accumulated since the early fifties from bremsstrahlung-[14-19], and electron-induced [20-24] fission experiments of non-actinide nuclei in the same energy region of the incident photon.

These photofission data have been generally interpreted on the basis of a model which considers the primary nuclear photoabsorption as taking place between the incoming photon and a neutron-proton pair (quasi-deuteron photoabsorption mechanism first proposed by Levinger [25]) followed by a competition between the process of nucleon evaporation and fission of the excited residual nucleus [4-8,11,26-28]. Since a collection of nearly two hundred experimental photofissility data is now available from the photofission experiments mentioned above ,we thought it worthwhile to perform a detailed systematic analysis of these data in the framework of the referred current photofission model. Due to the relatively high value for the fission barrier height ($\sim 20 - 50$ MeV)exhibited by all non-actinide nuclei [29], fissility (total fission probability, f) is expected to increase monotonously by one or more orders of magnitude from threshold on. The scope of the present analysis is, therefore, to give a detailed description of the fission behavior for ^{27}Al, ^{nat}Ti, ^{51}V, ^{154}Sm, ^{174}Yb, ^{nat}Hf, ^{181}Ta, ^{nat}W, ^{nat}Re, ^{nat}Os, ^{nat}Pt, ^{197}Au, ^{nat}Tl, ^{208}Pb, ^{nat}Pb, and ^{209}Bi target nuclei in the quasi-deuteron energy-range ($\sim 30 - 140$ MeV) of photonuclear absorption.

2 Calculation of nuclear photofissility

2.1 Simple model for photofission reactions

Following the generally accepted, current two-step model for intermediate-energy photofission reactions, the incoming photon is firstly absorbed by a neutron-proton pair, the incident energy being shared between these two nucleons. Depending on their final kinetic energies inside the nucleus soon after the primary interaction, one of these nucleons, or both, may, or may not, escape from the struck nucleus with a probability p, leading to a residual nucleus with a certain excitation energy E^* .In a second stage, after thermodynamic equilibrium is reached, fission will take place with a probability $P_f(E^*)$, as a result of a mechanism of competition between particle evaporation and fission experienced by the excited residual nucleus. Fissility is, therefore, obtained by multiplying these two referred probability values and summing up all possible modes of obtaining residual nuclei and of incident energy sharing between the neutron-proton pair.

Accordingly,for a target nucleus (Z, A) the following general formula has been deduced to calculate nuclear photofissility

$$f(k) = \frac{\int_{E_F^n}^{k+\frac{1}{5}(3E_F^n-2E_F^p)} \sum_{i=1}^{3} p_i(k, T_{n^*}) \times P_{f_i}^t(k, T_{n^*}) \mathrm{d}T_{n^*}}{k - \frac{2}{5}(E_F^n + E_F^p)} \ , \qquad (1)$$

Here, k is the incident photon energy; E_F^n and E_F^p are the Fermi energies, respectively, for neutrons and protons in the target nucleus ; $p_1 = \tau_n(1-\tau_p)$ is the probability of formation of the residual nucleus $(Z, A-1)$ with an excitation energy $E_1^* = k - T_{n*} + B_n$; $p_2 = \tau_p(1-\tau_n)$ is that for the residual nucleus $(Z-1, A-1)$ with excitation energy $E_2^* = k - T_{p*} + B_p$; $p_3 = (1-\tau_n) \times (1-\tau_p)$ is the probability of having the target nucleus itself with an excitation energy equal to the incident photon energy, i.e., $E_3^* = k$. The quantity $P_{f_i}^t$ represents the total fission probability for the different excited residual nuclei. In the above expressions, τ_n and τ_p denote, respectively, the probabilities of escaping for neutron and proton without suffering for any secondary interaction, i.e., the nuclear transparencies to neutron and proton; T_{n^*} and T_{p^*} are the kinetic energies, respectively, for neutron and proton in their final states (measured inside the target nucleus) after

absorption of the incoming photon by a neutron-proton pair; B_n and B_p are the binding energies, respectively, for neutron and proton. A fourth possibility there exists of obtaining residual nuclei, namely, escaping of both the neutron and proton simultaneously from the nucleus ($p_0 = \tau_n \tau_p$). In this case, however, no excitation energy is left to the residual nucleus $(Z-1, A-2)$, i.e., $E_0^* = 0$, with the consequence of null total fission probability for this residual.

Formula (1) has been obtained according to the following assumptions : i) the nucleus is considered to be a degenerate Fermi gas of non-interacting neutrons and protons confined within a spherically symmetric nuclear potential of radius R, the value of which is given by the equivalent root-mean-square radius of the nuclear charge distribution (see Table 1); ii) the angular distribution of the photointeraction with a quasi-deuteron (referred to the proton polar-angle in the center-of-mass system, θ'_p) is considered isotropic [28] . In addition, to calculate the kinetic energies T_{n^*} and T_{p^*}, the assumptions are made that: iii) neutrons and protons move at random in their respective Fermi gases ;iv) the kinetic energy distributions of neutrons and protons before the primary interaction are replaced by the respective average Fermi energies, in such a way that the initial kinetic energies are considered constant and equal to $T_n = T_p = (3/10)(E_F^n + E_F^p)$. As an example, Figure 1 shows the kinematics for a 100-MeV photointeraction $\gamma + (\mathrm{n} + \mathrm{p}) \rightarrow \mathrm{n}^* + \mathrm{p}^*$ in ^{184}W target nucleus.

From relativistic kinematics and the Pauli exclusion principle it results that the primary quasi-deuteron interaction can take place exclusively for photon energies $k > k_{qd} = (2/5)(E_F^n + E_F^p)$. On the other hand, retention of both neutron and proton occurs whenever the restrictions $T_{n^*} < E_c^n$ and $T_{p^*} < E_c^p$ are satisfied simultaneously, where E_c^n and E_c^p are the respective neutron and proton cut-off energies. Here, the E_c's are defined as the Fermi energy plus the binding energy of the loosest nucleon plus, in the case of proton, the Coulomb energy at the nuclear surface. Thus, retention of both neutron and proton after the primary photointeraction will occur for incident energies $k < k_r = (E_c^n + E_c^p) - (3/5)(E_F^n + E_F^p)$. As a consequence, in the incident energy interval $k_{qd} < k < k_r$ the residual nucleus formed is always the target nucleus ($p_3 = 1$) with

excitation energy $E^* = k$. For $k > k_r$ neutron and proton can be emitted simultaneously, but no excitation energy remains to the residual nucleus. Table 1 lists the values of the different nuclear quantities relevant to the present photofissility study.

2.2 Nuclear transparency

From the basic assumptions of the photofission reaction model outlined above it results that nuclear transparencies, which depend essentially on neutron and proton kinetic energies inside the nucleus, are the chief quantities to be used in evaluating in what proportion residual nuclei have been formed (and their respective excitation energies) following the quasi-deuteron photoabsorption. Different approaches have been developed in the past [32-36] to obtain closed formulae or to perform Monte Carlo calculations for the evaluation of nuclear transparencies to neutrons and protons produced within the nucleus. In the present analysis transparency-values to neutron and/or proton following the quasi-deuteron photointeraction have been calculated according to the formalism developed by de Carvalho *et al.* [28,34]. The method is based on the optical model and on the idea of an equivalent nucleus, i.e., a nucleus for which the transparency to a particle coming from outside is the same as the transparency to the same particle but emerging from inside the given nucleus. Figure 2 shows transparency-values for three representative target nuclei to emergent neutron (τ_{n^*}) and proton (τ_{p^*}) as a function of their kinetic energies ($T_{n^*} > E_c^n, T_{p^*} > E_c^p$) inside the nucleus. It has been found that the transparency-curves can be described to a good approximation (within $\sim 3\%$ on the average) by the general expression

$$\tau_i = \alpha + \beta\ T_i + \frac{\gamma}{T_i^4} \quad , i = \mathrm{n}^*,\ \mathrm{p}^*, \tag{2}$$

where α, β, γ (for neutron) and α', β', γ' (for proton) are parameters given by

$$\alpha = \tau_{n^*}^{min} - \frac{5\gamma}{T_{n^*}^{min^4}}\ , \tag{3}$$

$$\beta = \frac{4\gamma}{T_{n^*}^{min^5}}\ , \tag{4}$$

$$\gamma = \frac{\tau_{n^*}^c - \tau_{n^*}^{min}}{\frac{4E_c^n}{T_{n^*}^{min^5}} + \frac{1}{E_c^{n^4}} - \frac{5}{T_{n^*}^{min^4}}}\ , \tag{5}$$

and identical expressions are valid for proton, where the changes n* $\rightarrow$ p* and $E_c^n \rightarrow E_c^p$ are implicit. In the above expressions τ^c stands for the value of nuclear transparency at the cut-off energy, E_c, and τ^{min} for the minimum of nuclear transparency at the corresponding kinetic energy T^{min}. Table 2 lists, for the target nuclei considered in the present analysis, the values of the different parameters to calculate nuclear transparency according to Eq. (2). Figure 2 shows that nuclear transparencies first decrease with increasing particle energy. This behavior reflects the Pauli blocking effects on nucleon-nucleon cross section inside the nucleus causing, therefore, an increase in proton and/or neutron mean free path in nuclear matter at particles energies in the range $\sim$ 40–80 MeV (for details see [28]).

2.3 Average characteristics of the residual nucleus

In this section we present the routine calculation for the average values of the probability of formation of the residual nuclei after the primary photointeraction, $\bar{p}_i$, and the associated average excitation energies, $\bar{E}_i^*$, as a function of incident photon energy, k, for various target nuclei. From the definitions $p_0 = \tau_{n^*}\tau_{p^*}$, $p_1 = \tau_{n^*}(1-\tau_{p^*})$, $p_2 = \tau_{p^*}(1-\tau_{n^*})$, and $p_3 = (1-\tau_{n^*})(1-\tau_{p^*})$, with $\Sigma p_i = 1$ (see section 2.1), we have

$$\overline{p_o} = \frac{1}{d}\int_{E_F^n}^{\in - E_F^p} \tau_{n^*}(T_{n^*}) \cdot \tau_{p^*}(T_{p^*}) \mathrm{d}T_{n^*} \ , \tag{6}$$

$$\overline{p_1} = \frac{1}{d}\int_{E_F^n}^{\in - E_F^p} \tau_{n^*}(T_{n^*}) \mathrm{d}T_{n^*} - \overline{p_o} \ , \tag{7}$$

$$\overline{p_2} = \frac{1}{d}\int_{E_F^n}^{\in - E_F^p} \tau_{p*}(T_{p^*}) \mathrm{d}T_{n^*} - \overline{p_o} \ , \tag{8}$$

$$\overline{p_3} = 1 - \overline{p_0} - \overline{p_1} - \overline{p_2} \ , \tag{9}$$

where

$$d = k - (2/5)(E_F^n + E_F^p) \ , \ \in = k + (3/5)(E_F^n + E_F^p) \ . \tag{10}$$

Analytical, closed formulae to calculate the $\overline{p}_i$-values can be easily obtained by inserting the general expression (2) for the transparencies into Eqs. (6-9). As already discussed in

section 2.1, the associated excitation energy in the case of retention (no escaping) of both neutron and proton is simply $\overline{E}_3^* = k$, and for escaping of both nucleons it is $\overline{E}_0^* = 0$. For the other two cases we have

$$\overline{E}_1^* = k + B_n - \overline{T}_{n^*} \quad \text{and} \quad \overline{E}_2^* = k + B_p - \in + \overline{T}_{n^*} \tag{11}$$

(recall that $\in = T_{n^*} + T_{p^*}$). Now, the average $\overline{T}_{n^*}$ is calculated by using the p_1-values as weighted quantities, i.e.,

$$\overline{T}_{n^*} = \frac{\displaystyle\int_{E_F^n}^{\in - E_F^p} p_1 T_{n^*} \mathrm{d}T_{n^*}}{\displaystyle\int_{E_F^n}^{\in - E_F^p} p_1 \mathrm{d}T_{n^*}} \ , \tag{12}$$

which gives

$$\overline{T}_{n^*} = \frac{1}{d \cdot \overline{p}_1} \left[\int_{E_F^n}^{\in - E_F^p} \tau_{n^*}(T_{n^*}) T_{n^*} \mathrm{d}T_{n^*} - \int_{E_F^n}^{\in - E_F^p} \tau_{n^*}(T_{n^*}) \tau_{p^*}(T_{p^*}) T_{p^*} \mathrm{d}T_{n^*} \right] \ . \tag{13}$$

The trend of the average probability of excitation of residual nuclei which may be formed following the four routes discussed above, $\overline{p}_i (i = 0, 1, 2, 3)$, is shown in Figure 3 as a function of mass number of the target nucleus for a typical incident photon energy of $k = 100$ MeV. It is seen that the mode of excitation following retention of both nucleons, $\overline{p}_3$, is the most probable one in producing excited ($E_3^* = k$) residual nuclei ($\overline{p}_3$ is shown to be $\sim$ 2–3 times greater than the average of $\overline{p}_0$, $\overline{p}_1$, and $\overline{p}_2$). In Figure 4 are depicted the trends of $\overline{p}_i$ and $\overline{E}_i^* (i = 0, 1, 2, 3)$ as a function of incident photon energy for the representative target nucleus ^{154}Sm. Again, it is seen that not only the mode of excitation $i = 3$ reveals to be the most likely route to produce excited residual nuclei, but also the excitation left from the other three modes is either not much higher than the height of the fission barrier ($\sim$ 40 MeV in the present example) or null to produce a significant fission rate. Therefore, these three modes of formation of residual nuclei which involve escaping of neutron, proton, or both nucleons should not contribute significantly to fission in view of the small value of both formation probability and average excitation energy for these residuals. The same conclusions hold for the other non-actinide target nuclei. This result means that the contributions $p_1 P_{f_1}^t$ and $p_2 P_{f_2}^t$ to the summation in Eq. (1), although not negligible, are expected small, and may be though as within the

uncertainties of the $p_3 P^t_{f_3}$. Calculations have indicated indeed that for intermediate-mass and heavy pre-actinide nuclei ($A \geq 150$) the process in which $E^*_3 = k$ does contribute alone to more than 90 % of the total nuclear fissility; for less-massive nuclei of $A \leq 50$ excited at energies $E^* \gtrsim 100$ MeV the referred contribution amounts to more than 60 %, while at energies $E^* \lesssim 100$ MeV the process in which $E^*_3 = k$ contributes to 100 % of the total fissility. Thus, to a good approximation, Eq. (1) transforms into

$$f(k) \approx \frac{1}{d} \int_{E^n_F}^{\epsilon - E^p_F} p_3(k, T_{n^*}) \cdot P^t_{f_3}(k) \mathrm{d}T_{n^*} = \overline{p}_3(k) \cdot P^t_{f_3}(k) \ , \qquad (14)$$

i.e., fissility results to be given approximately by the total fission probability of the target nucleus excited to $E^*_3 = k$ times the average probability of formation of this residual, $\overline{p}_3(k)$. For practical purposes this latter quantity is, therefore, the relevant one in describing the quasi-deuteron photoexcitation which can lead the target nucleus to fission. Figure 5 shows the variation of $\overline{p}_3$ with incident photon energy for ^{27}Al, ^{48}Ti, ^{154}Sm, and ^{209}Bi target nuclei. The trends reflect the combined behavior of the nuclear transparencies to neutron and proton (cf. Figure 2) after the incident photon energy has been shared between these two nucleons. It is seen in Figure 5 that from a minimum around $\sim$ 50–70 MeV $\overline{p}_3$ increases with increasing photon energy at a rate which raises with the mass number. The conclusion can be drawn that heavy pre-actinide nuclei are more likely to be excited than intermediate-mass and less massive nuclei in the quasi-deuteron region of photoabsorption.

2.4 Total fission probability

The fission-evaporation competition process from an initial, excited residual nucleus ($Z, A, E^* = k$) is represented schematically in Figure 6. Along with neutron emission, proton and alpha-particle emissions may also compete, although to a lesser extent, with the fission mode. This is expected to occur especially when the height of the fission barrier is comparable with the Coulomb-plus-separation energy of the particle, as for $E^* \gtrsim 80$ MeV. Thus ,neutron emission, proton emission, alpha-particle emission, and fission are the competing modes for the de-excitation of the residual nucleus . The symbols in Figure 6 represent the probability values for the different de-excitation modes, where the numbers in sub-

scripts indicate the order of the different chance-fission or particle evaporation, i.e., f_1 is the first-chance fission probability, n_1 is the first-chance probability for neutron emission, p_1 is that for proton emission, $f_{3,pn}$ is the third chance-fission probability after successive emissions of one proton and one neutron, $\alpha_{2,n}$ is the second-chance probability for alpha-particle emission after the first neutron emission, and so forth. The total fission probability is given by

$$P_f^t(Z,A,E^*=k) = f_1 + n_1 f_{2,n} + p_1 f_{2,n} + \alpha_1 f_{2,\alpha} + \\ + n_1 n_{2,n} f_{3,2n} + n_1 p_{2,n} f_{3,np} + \cdots + p_1 n_{2,p} f_{3,pn} + \cdots + \alpha_1 n_{2,\alpha} f_{3,\alpha n} + \cdots \ . \quad (15)$$

The lowest limit for P_f^t is clearly f_1, because this quantity does not include the contributions from the subsequent chance-fission probabilities, i.e.,

$$P_f^t > f_1 \ . \quad (16)$$

Since generally fissility is given by $f \approx \overline{p} P_f^t$, where $\overline{p}$ is found in the range $\sim 0.34 - 1$ for non-actinide nuclei (cf. Eq. (14) and Figure 5), and P_f^t is expected to retain roughly the trend of the first-chance fission probability of residuals at any step of the evaporation chain ($P_{f_i}^t \propto f_{1_i}$), it follows that fissility, f_i, for a given residual i should be of the order of the first-chance fission probability, f_{1_i}. Results from a number of experiments have shown that the fissility of nuclei varies exponentially with both Z^2/A and E^* (see, for instance, [8], [10] and [37]). Therefore, by considering the first- as well as the successive higher-order-chance fission probabilities, and by noting that the probabilities for the same-order-chance fission are of the same order of magnitude, we can write from (15) that

$$P_f^t \approx f_1 + (1-f_1) f_2 + (1-f_1)(1-f_2) f_3 + \cdots \ . \quad (17)$$

An upper limit for P_f^t is obtained from Eq. (17) as

$$P_f^t \lesssim 3f_1 - 3f_1^2 + f_1^3 \quad (18)$$

by considering that the higher-order-chance fission probabilities should be nearly equal to or smaller than the first-chance one ($\cdots \lesssim f_3 \lesssim f_2 \lesssim f_1$), because excitation energy of the new residuals decreases progressively by ~ 10 MeV *per* particle evaporated.

Finally, by taking the average of the two limiting values expressed by Eqs. (16) and (18), and noting that $f_1 < 10^{-1}$ for the nuclei participating in the fission-evaporation competition process, it follows that the total fission probability can be approximated by

$$P_f^t \approx 2f_1 \ . \tag{19}$$

As a consequence the previous expression (14) to calculate fissility transforms into

$$f(k) \approx 2\overline{p}f_1 \ , \tag{20}$$

where the notation $P_{f_3}^t \approx 2f_1$ and $\overline{p}_3 \equiv \overline{p}$ is implicit. Equation (20) indicates that for non-actinide target (or residual) nuclei excited up to $E^* = k \approx 140$ MeV, fissility is expected to be nearly proportional to their first-chance fission probability. The uncertainty of ~ 25 % affecting the factor 2 can be incorporated into the uncertainties of both quantities $\overline{p}$ and f_1.

2.5 First-chance fission probability

The routine calculation for the evaporation-fission competition process, i.e., the calculation of the absolute probability-values for the first-chance neutron emission, proton emission, alpha-particle emission and fission , has been already detailed in [28]. The method is based on the statistical model proposed by Weisskopf [38] and Vandenbosch and Huizenga [39]. Accordingly, the first-chance fission (f_1), neutron emission (P_{n_1}), proton emission (P_{p_1}) and alpha-particle emission (P_{α_1}) probabilities are given by

$$f_1 = \frac{F}{1+F+G+H} \tag{21}$$

$$P_{n_1} = \frac{1}{1+F+G+H} \tag{22}$$

$$P_{p_1} = \frac{G}{1+F+G+H} \tag{23}$$

$$P_{\alpha_1} = \frac{H}{1+F+G+H} \ , \tag{24}$$

where F, G, and H denote, respectively, the probability of fission, proton emission, and alpha-particle emission relative to neutron emission. All these quantities are functions of Z, A and $E^* = k$ of the fissioning nucleus through the expressions given in [28]. The

nuclear quantities which appear explicitly in the expressions above are : i) total binding energy, B, ii) ground-state fission barrier, B_{f_0}, iii) neutron separation energy, B_n, iv) proton separation energy, B_p, v) alpha-particle separation energy, B_α, vi) Coulomb barrier at the nuclear surface for proton, V_{p_0}, and alpha-particle, V_{α_0}, vii) level-density parameter after neutron evaporation, a_n, and viii) ratio of the level-density parameter at the fission saddle point to a_n, $r = a_f/a_n$. For the competing alpha-emission channel a preformation probability of the alpha particle inside the nucleus has been assumed equal to one. As detailed in Refs. [8] and [37], we chose to evaluate the a_n-values using the expressions proposed by Iljinov *et al.* [40] on the basis of a statistical analysis of level densities of several hundred excited nuclides (Figure 7). V_{p_0}- and V_{α_0}-values have been calculated by the usual way [28]. The values for the quantities B, B_n, B_p, and B_α are those reported by Audi and Wapstra [31,41], while the B_{f_0}-values have been obtained from data reported in [29] and [42].

Since the final results of calculated fissility are very sensitive to the values of r, these have been determined in a semi-empirical way by assuming the photofission model described above and by making use of all available experimental data on total fission probability ($P_f^t = f_{exper}/\overline{p}$) for each fissioning nucleus [2-24]. In other words, semi-empirical r-values have been obtained by solving Eq. (20) in such a way that experimental fissility-values are reproduced. The solution for r reads

$$a\sqrt{r} - \ln\sqrt{r} = b \ , \tag{25}$$

where

$$a = \left\{4a_n k\left[1 - B_{f_0}\left(\frac{1}{k} - \frac{1}{B}\right)\right]\right\}^{1/2} \tag{26}$$

$$b = \ln\frac{4c}{15a\left(\frac{2}{P_f^t} - 1\right)} + \delta \tag{27}$$

$$c = (1 + G + H)A^{2/3}(k - B_n) \tag{28}$$

$$\delta = [4a_n(k - B_n)]^{1/2} \ , \tag{29}$$

which is valid for photon energies greater than $k_f = (B_{f_0}^{-1} + B^{-1})^{-1}$, or $k_f \approx B_{f_0}$.

For most of the target nuclei considered in the present work an experimental photofission cross section curve, σ_f, and/or a number of measured σ_f-points are available. In these cases the fissility-values have been deduced as $f_{exper} = \sigma_f/\sigma_a^T$, where σ_a^T is the total nuclear photoabsorption cross section which has been calculated by means of Levinger's modified quasi-deuteron model [28,43] . When only few experimental fissility points were available, an f-curve has been drawn through the points and extended towards the low-energy ($\sim 40-50$ MeV) region following the general trend of f versus k (see, for instance, [12]). It has been found that the r-values obtained as described above could be fitted to a general formula of the type

$$r = 1 + \frac{p}{k^q} \ , \tag{30}$$

where $p > 0$ and $q > 0$ are constant to be determined by the least-squares method to r-values of a given target nucleus. Table 3 lists the values of parameters p and q, the number of semiempirical r-values used in each fitting procedure, n, as well as the values of k_f. Finally, Figure 8 shows the trend of r *versus* the incident photon energy (excitation energy) for some of these nuclei. The asymptotical value towards $r \approx 1$ observed for all nuclei is compatible with the phenomenological systematics of level density by Iljinov *et al.* [40] as well as with the theoretical estimations reported by Ignatyuk *et al.* [44] and Rostopchin et al. [45]. Only for ^{182}W target nucleus the experimental σ_f-data [24] did not lead to r-values compatible with the trend defined by (30) (the value of parameter q resulted negative). The fitted r-values have been subsequently applied to compare calculated fissility-values with 182 experimental data (see below). We remark that the number of experimental data available up to now (and of target nuclei thus considered in the present analysis) is still small to obtain a completely smooth correlation of parameter r with mass number over the entire mass region from Al to Bi.

3 Results and Discussion

3.1 First-chance probabilities for particle emission and fission

Among the various target nuclei considered in the present photofission reaction study (Table 1) we chose ^{51}V, ^{174}Yb, and ^{197}Au as representative nuclei to illustrate the calculated trends of P_{n_1}, P_{p_1}, P_{α_1}, and f_1 with excitation energy (or incident photon energy) as they are given by Eqs. (21-24) . These nuclei have been chosen on the basis of the marked differences between the values for their ground-state fission barrier, namely $\sim$ 53 MeV for ^{51}V, $\sim$ 32 MeV for ^{174}Yb, and $\sim$ 22 MeV for ^{197}Au. The results depicted in Figure 9 show that in all cases the first-chance fission probability (f_1) increases steeply at low energies , and exhibits an asymptotic-like behavior as nuclear excitation increases from $\sim$ 80 MeV on. The values of the first-chance fission probability are seen to vary by four or six orders of magnitude as the excitation energy increases up to $\sim$ 140 MeV. Figure 9 shows also that neutron emission predominates ($P_{n_1} \approx 1$) over the other modes of de-excitation for both ^{174}Yb and ^{197}Au residuals, while for ^{51}V neutron evaporation competes approximately to the same extent with proton emission. In general, for intermediate-mass and less massive nuclei, charged-particle evaporation predominates over fission, whereas for heavy pre-actinide nuclei some degree of competition between charged particles and fission is apparent. All these features seem to reflect the influence of the different barrier heights on the competition between proton and alpha-particle emission modes and fission , for excited fissioning systems.

3.2 Nuclear photofissility

The calculated trends of photofissility for the nuclei considered in the present analysis are obtained from the expressions

$$f(k) = 2f_1(k), \begin{cases} k_f < k < k_r \quad \text{and} \quad 6 < Z^2/A < 29.5 \\ k_{qd} < k < k_r \quad \text{and} \quad 29.5 < Z^2/A < 33 \end{cases} \tag{31}$$

or

$$f(k) = 2\overline{p}_3(k) \times f_1(k) \ , \ k_r < k \lesssim 140 \text{ MeV} \quad \text{(all nuclei)} \ . \tag{32}$$

The f-curves for the various nuclei are reported in Figs. 10-14 (full lines) , together with the experimental data (points) . The overall average uncertainty of the calculated fissility-curves has been estimated in the range $\sim 30 - 40\%$. In general the calculated trends fit satisfactorily well the experimental data in the entire region of incident photon energy. Some disagreement is noted, however, in a few cases as for ^{27}Al at 40 MeV (Figure 10), ^{181}Ta at 69, 130, and 140 MeV (Figure 12-b), ^{nat}Pt at 110 MeV (Figure 13-b), ^{197}Au at 60 and 64 MeV (Figure 13-c), ^{208}Pb at 30 and 40 MeV (Figure 14-a), ^{nat}Pb at 60 and 64 MeV (Figure 13-e), and ^{209}Bi at 26 and 64 MeV (Figure 14-b), where differences between calculated and experimental values amount to a factor greater than ~ 5. Such a discrepancy may be ascribed mainly to experimental difficulties in measuring very low fissility-values at energies $k \lesssim 80$ MeV, and/or in obtaining a better dependence of the quantity $r = a_f/a_n$ on excitation energy.

Two striking features have been evidenced from the present analysis . The first one is that fissility increases by orders of magnitude from the lower energies on. The enhancement of the fission channel arises from an increase of the probability of nuclear excitation, $\overline{p}_3$, combined with a lowering of the height of the fission barrier with increasing of the incident photon energy (or excitation). The second one is that the behavior of nuclear fissility with photoexcitation comes mainly from the strong dependence of f upon the energy-related variation of both the fission barrier, $B_f = B_{f_0}(1 - E^*/B)$, and the level-density parameters, a_n and a_f (or the ratio $r = a_f/a_n$) (cf. Figures 7 and 8). This can be easily understood by writing for fissility the approximate expression $f \simeq C\mathrm{e}^D$, where

$$C \simeq \frac{15\overline{p}_3}{A^{2/3}(E^* - B_n)} \left[\frac{a_n(E^* - B_f)}{r}\right]^{1/2} \tag{33}$$

is a quantity which does not vary significantly with the excitation energy, while

$$D = 2a_n^{1/2}[r^{1/2}(E^* - B_f)^{1/2} - (E^* - B_n)^{1/2}] \tag{34}$$

exhibits a quite linear dependence with E^* (or k) for energies above about 90 MeV. This means that for nuclei which are more difficult to break up into two fragments of comparable masses ,the exit channels for particle emission become much more important (especially the neutron emission channel) than the fission one. We remark that the essential physical

basis that explains in a satisfactory way the main features of the analysed photofission reactions is ; i) the predominance of the mode of formation of residual nuclei of average characteristics $\overline{Z}^* = Z$, $\overline{A}^* = A$, and $\overline{E}^* = k$ after the fast photoabsorption stage ; ii) the approximation $P_f^t \simeq 2f_1$ to include the first- and higher-order-chance fission probabilities during the low stage of de-excitation of the residuals where particle emission (n , p, α) and fission compete.

3.3 Photofissility *versus* parameter Z^2/A

The present systematic analysis of photofissility provides also information concerning the variation of nuclear fissility for a number of target nuclei of unknown r-values. Two different target mass regions may be defined where r-values are seen to vary smoothly with mass number (or Z^2/A), namely, the region of less-massive nuclei (Al–Ti, $6 \lesssim Z^2/A \lesssim 10$), and the region of pre-actinide and intermediate-mass nuclei (Sm–Bi, $25 \lesssim Z^2/A \lesssim 33$). Within the large uncertainties expected in the calculated fissility-values (up to a factor 2) the present model can be applied to predict fissility of nuclei to the referred mass region. Firstly, we construct smooth trends of $r = a_f/a_n$ with Z^2/A from the r-values determined semiempirically for the sixteen target nuclei analysed in the present work (Eq. (30) and Table 3). Results are shown in Figure 15 for 60-, 100-, and 140-MeV of excitation (full lines). Next, values of r have been estimated from these trends for nuclei along the beta-stability valley to both mass regions. Since there not exist photofissility data for nuclei in the intermediate-mass region of $10 \lesssim Z^2/A \lesssim 25$, we decided, as a first, rough approximation, to interpolate a linear dependence of r *versus* Z^2/A for this region of mass (dashed line in Figure 15). Of course the uncertainty associated with the r-values estimated in this way are not small ($15 - 20$ %), for the pairing and/or shell effects have been not included at all. Figure 16 shows the resulting fissility dependence on Z^2/A at the three photon energy-values mentioned and for nuclei ranging from Al to Po. Actinide target nuclei were not included in the present study, for they have been recently analysed in a quite complete, comprehensive investigation (from both the experimental and theoretical points of view) on photofission reactions at photon energies in the range 68–264 MeV by Sanabria *et al.* [46]. The main features from Figure 16

are here pointed out: i) the presence of relative minima of fissility in the region Rb–Pr ($16.0 \lesssim Z^2/A \lesssim 24.5$) is evident , and these minima seem to indicate the effect of the relative maxima of the ground-state fission barrier in the vicinity of $N = 50$, $Z = 50$, and $N = 82$ shell closures [8]); ii) shell effects are seen also to manifest around other shell closures , especially in the vicinity of the double magic ^{208}Pb target nucleus excited to 60 MeV, as already discussed in [7]; iii) in general, the trend exhibited by fissility is essentially an inverse reflection of that showed by the fission barrier [29], i.e., fissility should increase as Z^2/A decreases from about 16 or so; iv) finally, it is clearly seen from Figure 16 that the distance between successive f-curves diminishes as the incident photon energy increases. We remark that within the referred limitations imposed by the assumptions of the model as well as the scarcity and quality of the available data, the present calculation model can be used to predict photofission cross section (or photofissility) either of known nuclei at unmeasured energies or nuclei not yet investigated in the energy range $\sim 30 - 140$ MeV of photonuclear absorption. Results in Figure 16 represent, therefore, only an approximate dependence of photofissility on both Z^2/A and nuclear excitation, especially in the region of nuclei of $10 \lesssim Z^2/A \lesssim 25$, where the semiempirical dependence of r with Z^2/A is unknown.

4 Summary and Conclusion

In the course of the present work, experimental photofission data for sixteen target nuclei ranging from Al to Bi at incident energies covering the quasi-deuteron region of photonuclear interaction ($\sim$ 30–140 MeV) have been analysed and interpreted on the basis of the current, two-step model for photofission reactions. The model considers a rapid, primary photointeraction with neutron-proton pairs leading to an excited residual nucleus which, subsequently, de-excite by a process of competition between fission and particle evaporation. Nuclear transparencies to neutron and proton have shown to be the chief quantities in defining the average characteristics of the residual nuclei, and also in what proportion these residuals have been formed after the quasi-deuteron photoabsorption process. It has been shown that the most probable and also significant mode of excitation which leads

the nucleus to fission is that in which both neutron and proton in their final states are retained inside the nucleus, i.e., the residual is the target nucleus excited to $E^* = k$.

During the de-excitation process we have considered the neutron, proton, and alpha particle emission channels to compete with the fission one. Besides, the higher-order chance fission probabilities have been taken into account through the approximation that the total fission probability of a given residual equals twice the first-chance fission probability of this residual ($P_f^t \approx 2f_1$). In the evaporation-fission competition routine we have used for the level density parameter a_n an updated expression proposed by Iljinov *et al.* [40], which incorporates corrections due to excitation energy and shell effects as well. Since the values for the ratio $r = a_f/a_n$ are not well defined in the literature, and the resulting calculated fissility is very sensitive to the r-values, we decided to determine the ratio $r = a_f/a_n$ in a semiempirical way by assuming the photofission model summarized above and by making use of the available experimental photofissility data. In other words, the quantity a_f/a_n has been treated as an adjustable model-parameter characterized by the trend of monotonous decreasing with increasing excitation energy, and reaching asymptotical values towards ~ 1.

Fissility curves obtained from the above routine calculation are found to fit the experimental data rather satisfactorily for all nuclei analyzed in the present work. Finally, the variation of photofissility with parameter Z^2/A has exhibited not only an inverse correlation of fissility with the height of the fission barrier for nuclei along the beta-stability valley, but also an apparent influence of shell effects on calculated fissility, especially at energies below ~ 80 MeV.

In spite of the uncertainties associated with the values of the different quantities and parameters which enter into the calculations, the model developed in the present analysis seems capable to explain in a satisfactory way the main features of photofissility of complex nuclei at incident energies in the range $\sim$ 30–140 MeV.

Acknowledgments

The authors wish to express their gratitude to the Italian INFN (Sezione di Roma 2) and the Brazilian CNPq and CNEN for partial supporting of this work.

References

[1] D. Babusci, V. Bellini, M. Capogni, L. Casano, A. D'Angelo, F. Ghio, B. Girolami, L. Hu, D. Moricciani, and C. Schaerf, Riv. Nuovo Cimento **19** (1996).

[2] H. -D. Lemke, B. Ziegler, M. Mutterer, J. P. Theobald, and N. Cârjan, Nucl. Phys. **A342**, 37 (1980).

[3] V. Bellini, V. Emma, S. Lo Nigro, C. Milone, G. S. Pappalardo, E. De Sanctis, P. Di Giacomo, C. Guaraldo, V. Lucherini, E. Polli, and A. R. Reolon, Lettere Nuovo Cimento **36**, 587 (1983).

[4] C. Guaraldo, V. Lucherini, E. De Sanctis, P. Levi Sandri, E. Polli, A. R. Reolon, S. Lo Nigro, S. Aiello, V. Bellini, V. Emma, C. Milone, and G. S. Pappalardo, Phys. Rev. C **36**, 1027 (1987).

[5] J. B. Martins, E.L. Moreira, O. A. P. Tavares, J. L. Vieira, J. D. Pinheiro Filho, R. Bernabei, S. D'Angelo, M. P. De Pascale, C. Schaerf, and B. Girolami, Nuovo Cimento **A101**, 789 (1989).

[6] V. Lucherini, C. Guaraldo, E. De Sanctis, P. Levi Sandri, E. Polli, A. R. Reolon, A. S. Iljinov, S. Lo Nigro, S. Aiello, V. Bellini, V. Emma, C. Milone, G. S. Pappalardo, and M. V. Mebel, Phys. Rev. C **39**, 911 (1989).

[7] J. B. Martins, E. L. Moreira, O. A. P. Tavares, J. L. Vieira, L. Casano, A. D'Angelo, C. Schaerf, M. L. Terranova, D. Babusci, and B. Girolami, Phys. Rev. C **44**, 354 (1991).

[8] O. A. P. Tavares, J. B. Martins, E. L. Moreira, M. L. Terranova, M. Capogni, L. Casano, A. D'Angelo, D. Moricciani, C. Schaerf, B. Girolami, F. Ghio, and D. Babusci, J. Phys. G: Nucl. Part. Phys. **19**, 2145 (1993).

[9] O. A. P. Tavares, J. B. Martins, E. de Paiva, E. L. Moreira, J. L. Vieira, M. L. Terranova, M. Capogni, L. Casano, A. D'Angelo, D. Moricciani, F. Ghio, B. Girolami, and D. Babusci, J. Phys. G: Nucl. Part. Phys. **19**, 805 (1993).

[10] M. L. Terranova, O. A. P. Tavares, G. Ya. Kezerashvili, V. A. Kiselev, A. M. Milov, N. Yu. Muchnoi, A. I. Naumenkov, V. V. Petrov, I. Ya. Protopopov, E. A. Simonov, E. de Paiva, and E. L. Moreira, J. Phys. G: Nucl. Part. Phys. **22**, 511 (1996).

[11] M. L. Terranova, G. Ya. Kezerashvili, V. A. Kiselev, A. M. Milov, S. I. Mishnev, I. Ya. Protopopov, V. N. Rotaev, D. N. Shatilov, and O. A. P. Tavares, J. Phys. G: Nucl. Part. Phys. **22**, 1661 (1996).

[12] M. L. Terranova, G. Ya. Kezerashvili, A. M. Milov, S. I. Mishnev, N. Yu. Muchnoi, A. I. Naumenkov, I. Ya. Protopopov, E. A. Simonov, D. N. Shatilov, O. A. P. Tavares, E. de Paiva, and E. L. Moreira, J. Phys. G: Nucl. Part. Phys. **24**, 205 (1998).

[13] O. A. P. Tavares, E. de Paiva, G. Ya. Kezerashvili, R. Ya. Kezerashvili, N. Yu. Muchnoi, A. I. Naumenkov, I. Ya. Protopopov, E. A. Simonov, and M. L. Terranova, J. Phys. G: Nucl. Part. Phys. **25**, 1979 (1999).

[14] G. Bernardini, R. Reitz, and E. Segré, Phys. Rev. **90**, 573 (1953).

[15] J. A. Jungerman and H. M. Steiner, Phys. Rev. **106**, 585 (1957).

[16] E. V. Minarik and V. A. Novikov, J. Exptl. Theoret. Phys. (USSR) **32**, 241 (1957) [Sov. Phys. JETP **5**, 253 (1957)].

[17] Yu. N. Ranyuk and P. V. Sorokin, J. Nucl. Phys. (USSR) **5**, 37 (1967) [Sov. J. Nucl. Phys. **5**, 26 (1967)].

[18] A. V. Mitrofanova, Yu. N. Ranyuk, and P. V. Sorokin, Yad. Fiz. **6**, 703 (1967) [Sov. J. Nucl. Phys. **6**, 512 (1968)].

[19] R. V. Warnock and R. C. Jensen, J. Inorg. Nucl. Chem. **30**, 2011 (1968).

[20] L. G. Moretto, R. C. Gatti, S. G. Thompson, J. T. Routti, J. R. Heisenberg, L. M. Middleman, M. R. Yearian, and R. Hofstadter, Phys. Rev. **179**, 1176 (1969).

[21] J. D. T. Arruda-Neto, M. Sugawara, T. Tamae, O. Sasaki, H. Ogino, H. Miyase, and K. Abe, Phys. Rev. C **31**, 2331 (1985); **34**, 935 (1986).

[22] J. D. T. Arruda-Neto, M. Sugawara, H. Miyase, T. Kobayashi, T. Tamae, K. Abe, M. Nomura, H. Matsuyama, H. Kawahara, K. Namai, M. L. Yoneama, and S. Simionatto, Phys. Rev. C **41**, 354 (1990).

[23] J. D. T. Arruda-Neto, T. Saito, M. Sugawara, T. Tamae, H. Miyase, K. Abe, K. Takahisa, O. Konno, M. Oikawa, and S. Simionatto, Phys. Rev. C **48**, 1594 (1993).

[24] J. D. T. Arruda-Neto, T. Saito, M. Sugawara, T. Tamae, H. Miyase, K. Abe, O. Konno, M. Oikawa, A. Deppman, S. Simionatto, E. M. L. Macedo, and B. S. Bhandari, Phys. Rev. C **51**, R452 (1995).

[25] J. S. Levinger, Phys. Rev. **84**, 43 (1951).

[26] A. S. Iljinov, E. A. Cherepanov, and S. E. Chigrinov, Yad. Fiz. **32**, 322 (1980) [Sov. J. Nucl. Phys. **32**, 166 (1980)].

[27] C. Guaraldo, V. Lucherini, E. De Sanctis, A. S. Iljinov, M. V. Mebel, and S. Lo Nigro, Nuovo Cimento **A103**, 607 (1990).

[28] O. A. P. Tavares and M. L. Terranova, Z. Phys. A **343**, 407 (1992).

[29] W. D. Myers and W. J. Swiatecki, Nucl. Phys. **81**, 1 (1966).

[30] I. Angeli, International Nuclear Data Committee-INDC (HUN)-033, IAEA-NDS (September, 1999).

[31] G. Audi and A. H. Wapstra, Nucl. Phys. **A565**, 66 (1993).

[32] K. A. Brueckner, R. Serber, and K. M. Watson, Phys. Rev. **84**, 258 (1951).

[33] B. Forkman and B. Schröder, Phys. Scripta **5**, 105 (1972).

[34] H. G. de Carvalho, J. B. Martins, O. A. P. Tavares, R. A. M. S. Nazareth, and V. di Napoli, Lett. Nuovo Cimento **2**, 1139 (1971).

[35] N. L. Emets, G. Ya. Lyubarskii, Yu. N. Ranyuk, and P. V. Sorokin, Preprint KhFTI 72–37. Khar'kov Physico-Technical Institute (1972); N. L. Emets, V. I. Noga, G. D.

Pugacev, and Yu. N. Ranyuk, Preprint VDK 539–172-3, Khar'kov Physico-Technical Institute (1973).

[36] A. Leprête, H. Beil, R. Bergère, P. Carlos, J. Fagot, A. Veyssière, and I. Halpern, Nucl. Phys. A **390**, 221 (1982).

[37] M. L. Terranova, G. Ya. Kezerashvili, V. A. Kiselev, A. M. Milov, S. I. Mishnev, I. Ya. Protopopov, V. N. Rotaev, D. N. Shatilov, and O. A. P. Tavares, Preprint Notas de Física CBPF-NF–38/96, Centro Brasileiro de Pesquisas Físicas–CBPF, Rio de Janeiro (July, 1996), unpublished.

[38] V. F. Weisskopf, Phys. Rev. **52**, 295 (1937).

[39] R. Vandenbosch and J. R. Huizenga, in *Nuclear Fission* (1^{st} edition, pp. 227, New York: Academic Press 1973).

[40] A. S. Iljinov, M. V. Mebel, N. Bianchi, E. De Sanctis, C. Guaraldo, V. Lucherini, V. Muccifora, E. Polli, A. R. Reolon, and P. Rossi, Nucl. Phys. **A543**, 517 (1992).

[41] G. Audi and A. H. Wapstra, Nucl. Phys. **A565**, 1 (1993).

[42] W. D. Myers, in *Droplet Model of Atomic Nuclei* (1^{st} Edition, pp. 35, New York: Plenum Press, 1977).

[43] J. S. Levinger, Phys. Lett. **B82**, 181 (1979).

[44] A. V. Ignatyuk, M. G. Itkis, V. N. Okolovich, G. N. Smirenkin, and A.S. Tishin, Yad. Fiz. **21**, 1185 (1975) [Sov. J. Nucl. Phys. **21**, 612 (1975)].

[45] E. M. Rostopchin, Yu. B. Ostapenko, M. I. Svirin, and G. N. Smirenkin, Yad. Fiz. **49**, 24 (1989) [Sov. J. Nucl. Phys. **49**, 15 (1989)].

[46] J. C. Sanabria, B. L. Berman, C. Cetina, P. L. Cole, G. Feldman, N. R. Kolb, R. E. Pywell, J. M. Vogt, V. G. Nedorezov, A. S. Sudov, and G. Ya. Kezerashvili, Phys. Rev. C **61**, 034604 (2000).

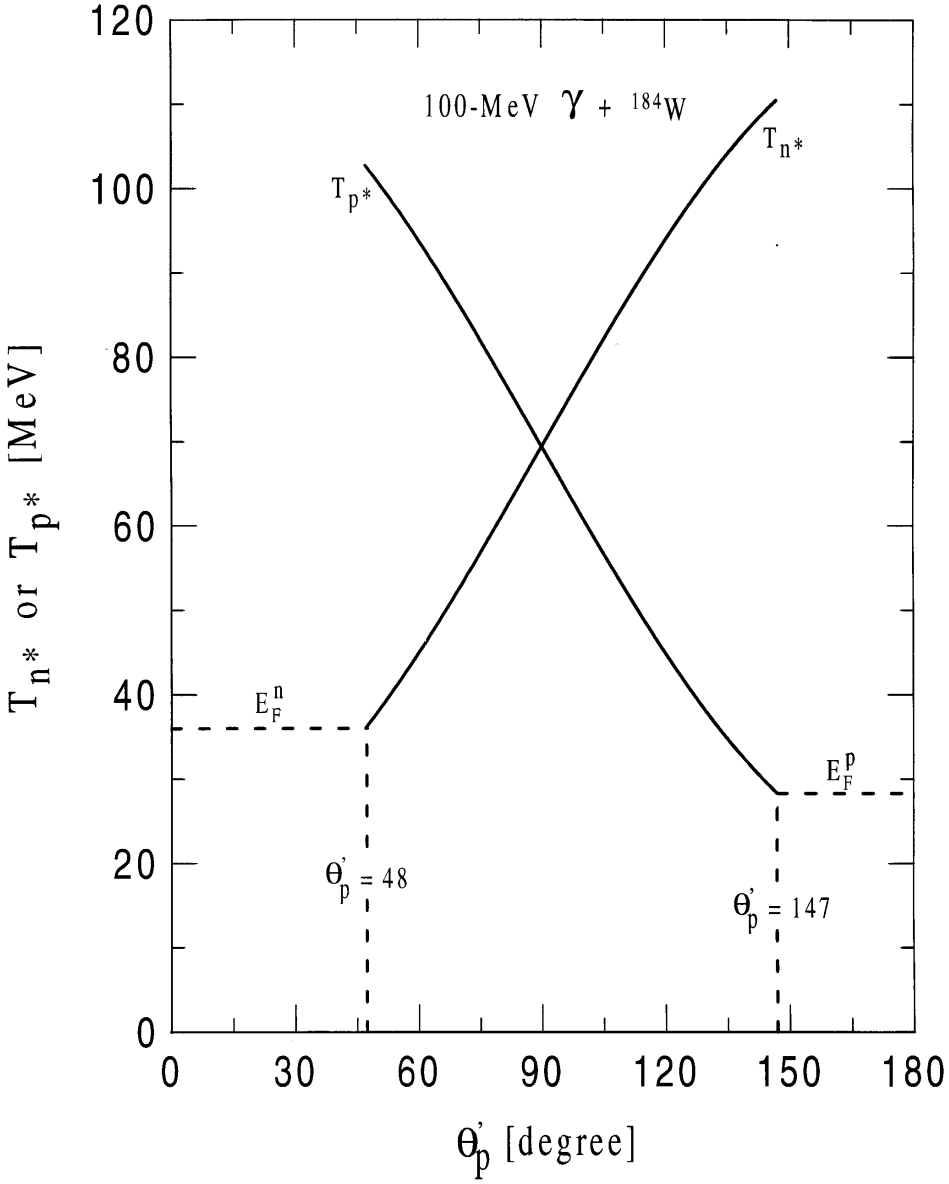
100-MeV γ + 184W
Tn*
Tp*
En F
Ep F
θ'p = 48
θ'p = 147
Tn* or Tp* [MeV]
θ'p [degree]
0
20
40
60
80
100
120
0
30
60
90
120
150
180

Fig. 1

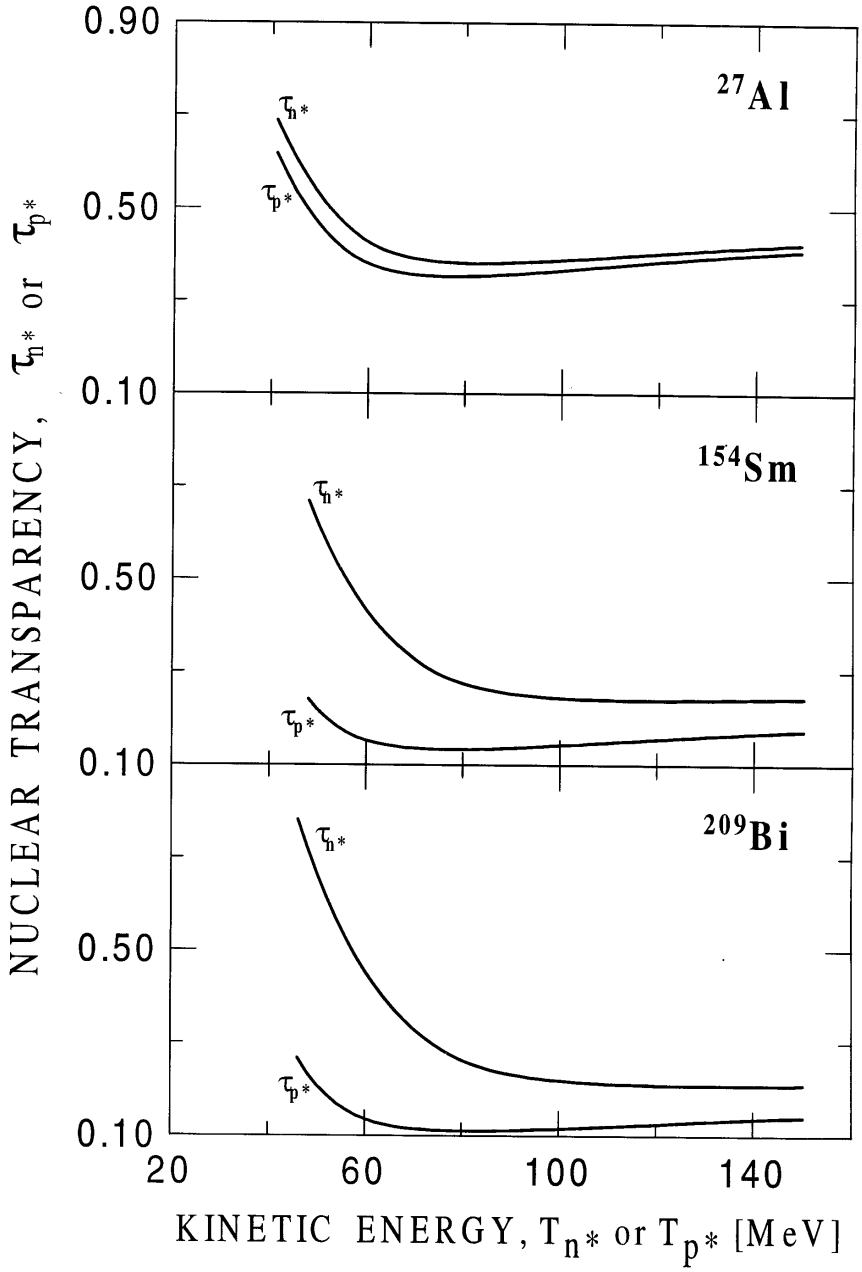
0.90
0.50
0.10
^{27}Al
τ_{n*}
τ_{p*}
^{154}Sm
^{209}Bi
NUCLEAR TRANSPARENCY, τ_{n*} or τ_{p*}
20
60
100
140
KINETIC ENERGY, T_{n*} or T_{p*} [MeV]

Fig. 2

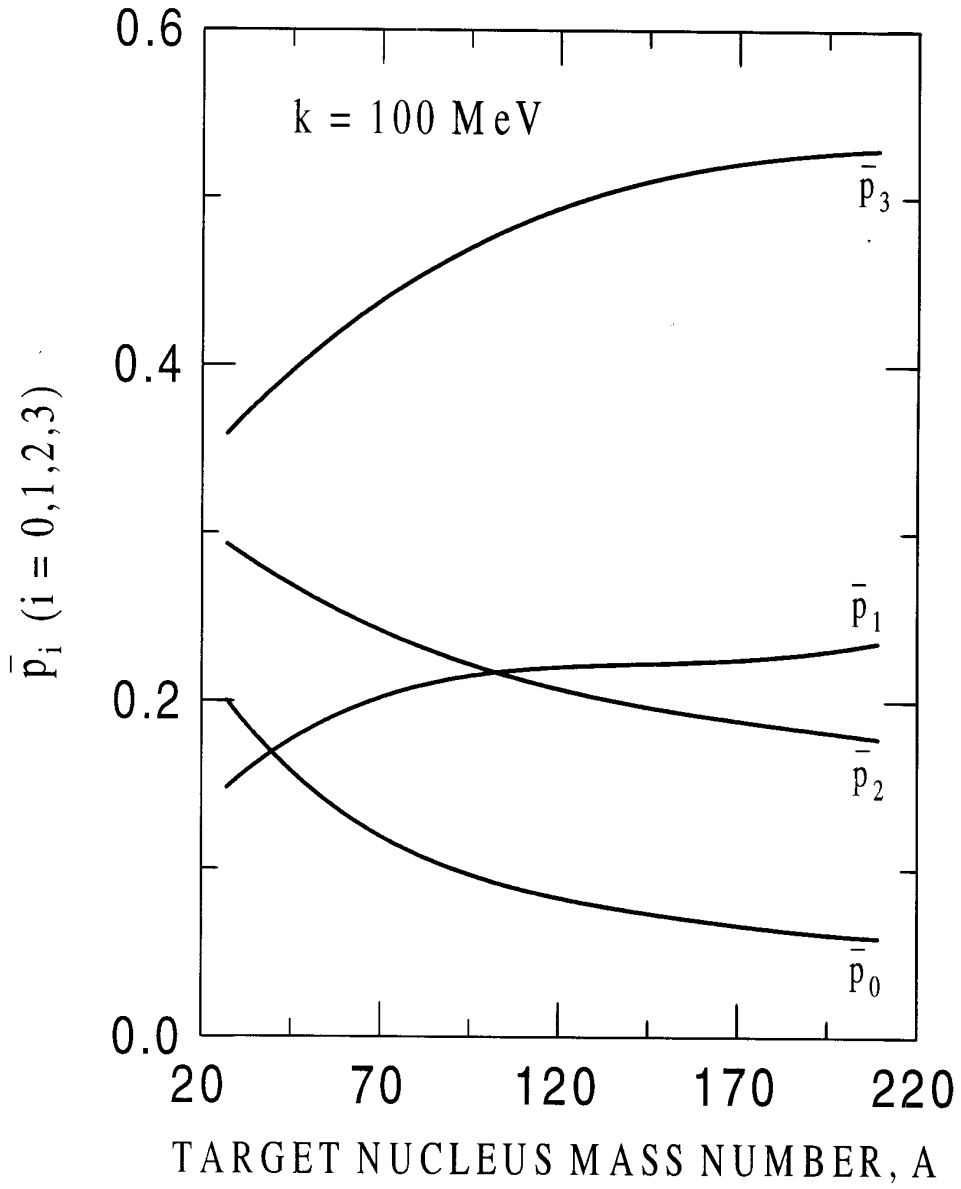
0.6
0.4
0.2
0.0
k = 100 MeV
$\bar{p}_3$
$\bar{p}_1$
$\bar{p}_2$
$\bar{p}_0$
$\bar{p}_i$ (i = 0,1,2,3)
20
70
120
170
220
TARGET NUCLEUS MASS NUMBER, A

Fig. 3

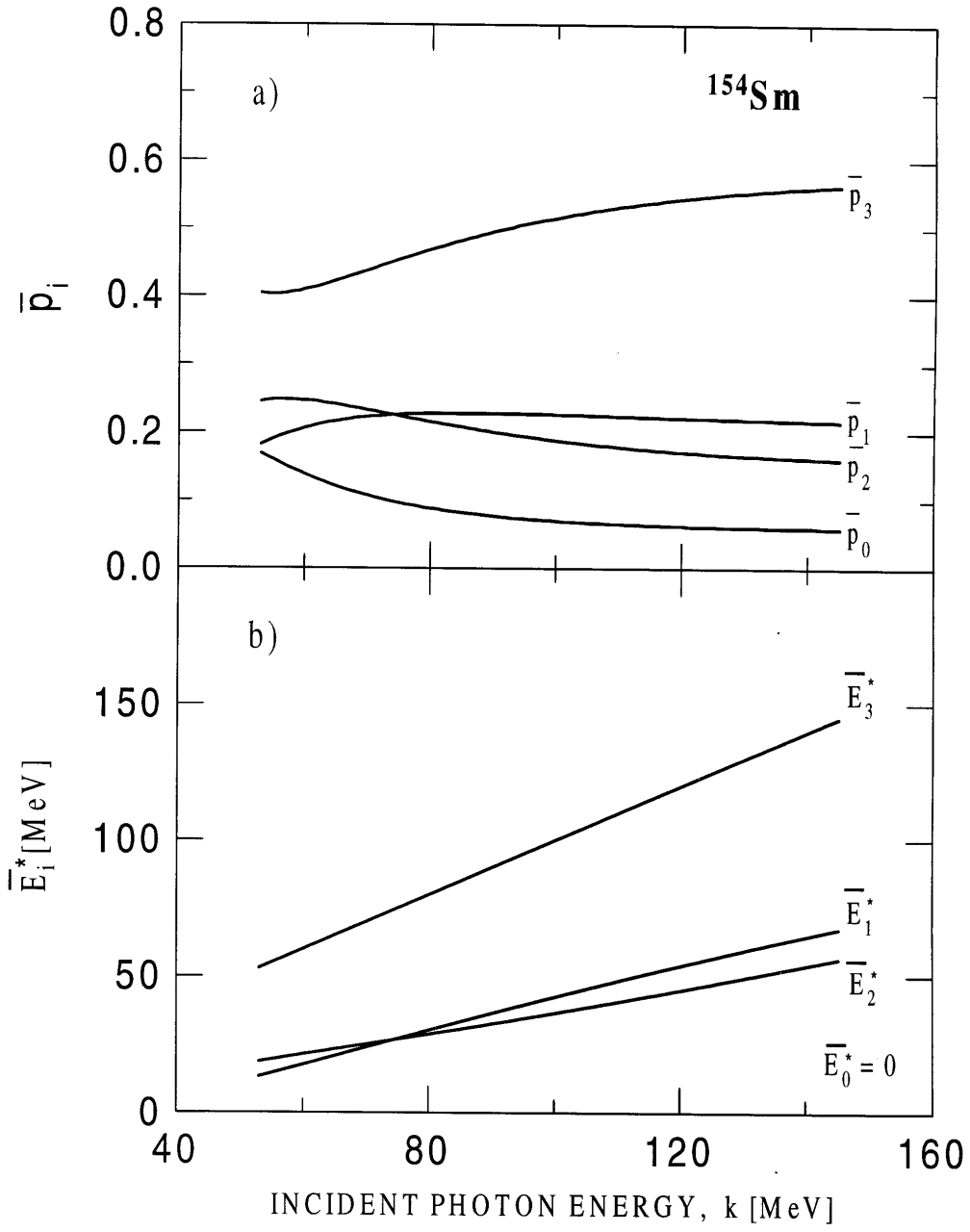
a)
^{154}Sm
$\bar{p}_3$
$\bar{p}_1$
$\bar{p}_2$
$\bar{p}_0$
$\bar{p}_i$
0.8
0.6
0.4
0.2
0.0
b)
$\bar{E}_3^*$
$\bar{E}_1^*$
$\bar{E}_2^*$
$\bar{E}_0^* = 0$
$\bar{E}_i^*$[MeV]
150
100
50
0
40
80
120
160
INCIDENT PHOTON ENERGY, k [MeV]

Fig. 4

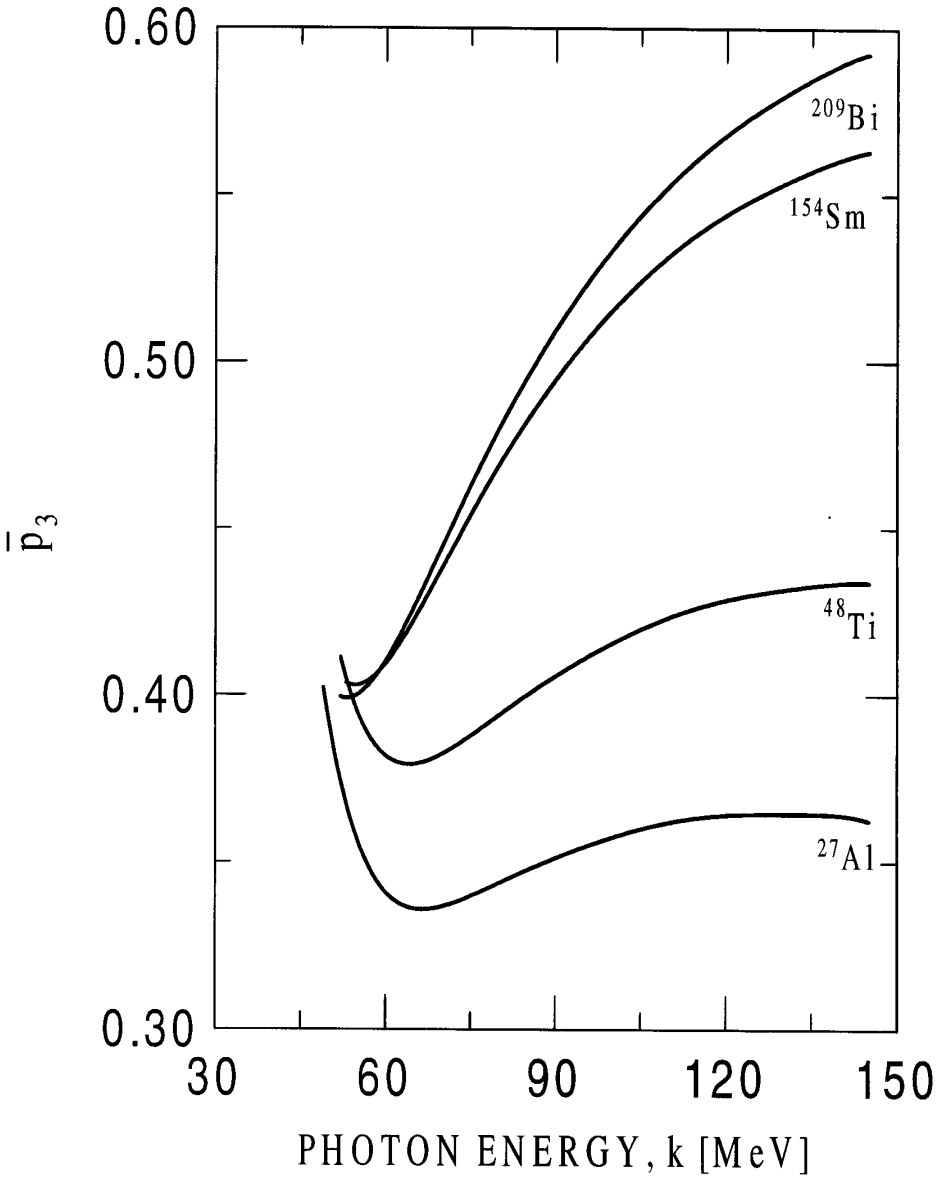
0.60
0.50
0.40
0.30
$\bar{p}_3$
^{209}Bi
^{154}Sm
^{48}Ti
^{27}Al
30
60
90
120
150
PHOTON ENERGY, k [MeV]

Fig. 5

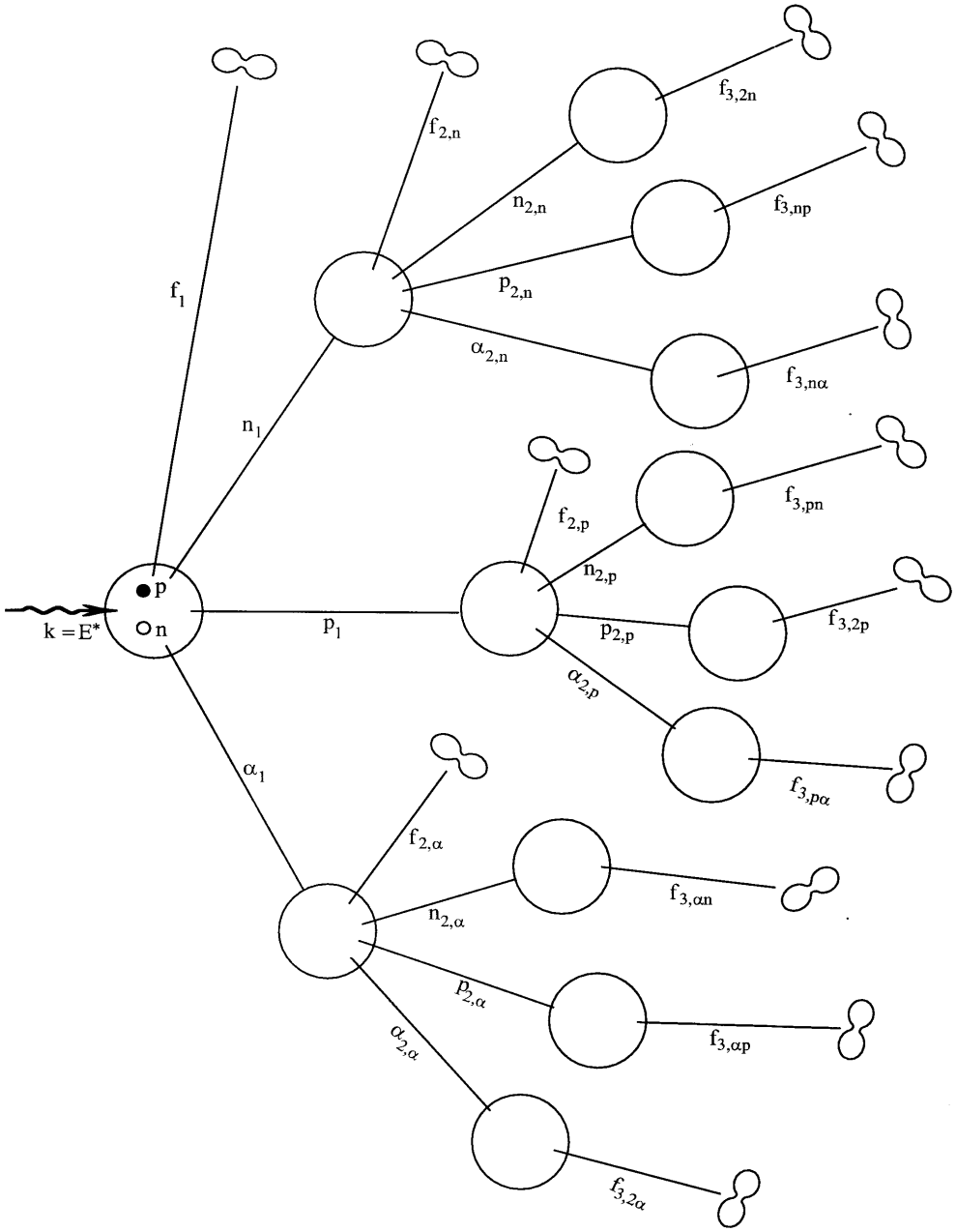
f1
f2,n
f3,2n
n2,n
f3,np
p2,n
α2,n
f3,nα
n1
f2,p
f3,pn
n2,p
p
k = E*
n
p1
p2,p
f3,2p
α2,p
f3,pα
α1
f2,α
f3,αn
n2,α
p2,α
f3,αp
α2,α
f3,2α

Fig. 6

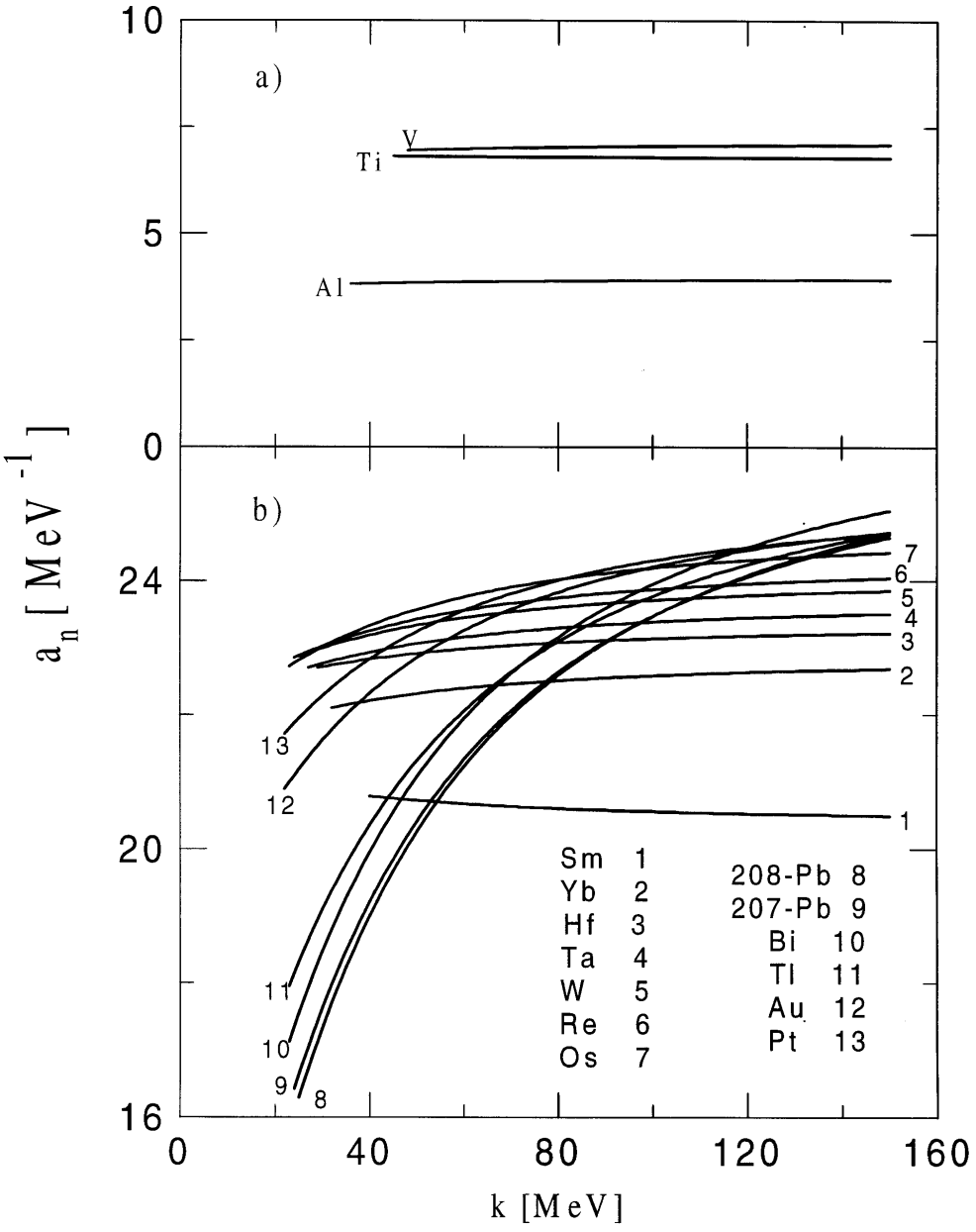
a)
V
Ti
Al
b)
a_n [MeV^{-1}]
k [MeV]
Sm 1
Yb 2
Hf 3
Ta 4
W 5
Re 6
Os 7
208-Pb 8
207-Pb 9
Bi 10
Tl 11
Au 12
Pt 13

Fig. 7

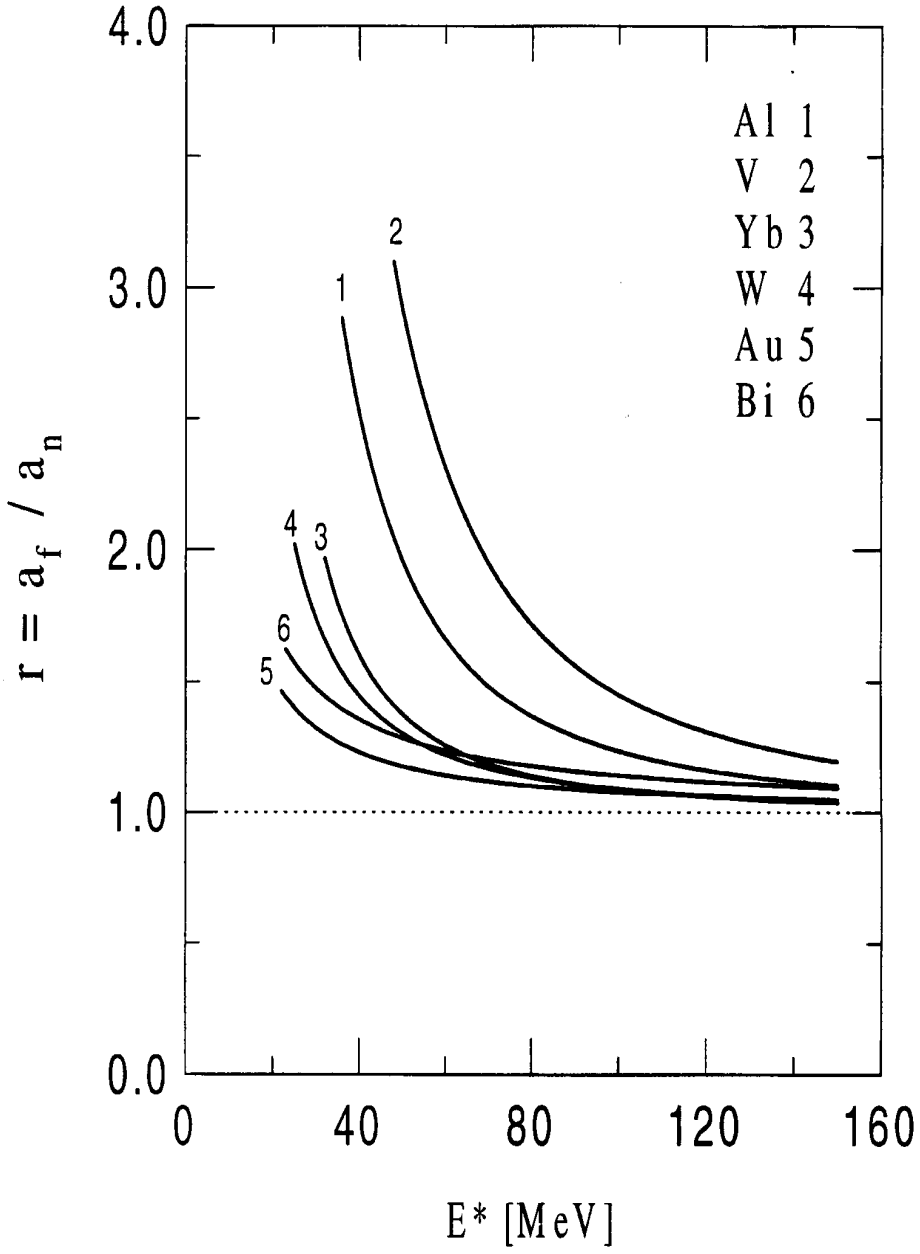
4.0
3.0
2.0
1.0
0.0
0
40
80
120
160
r = a_f / a_n
E* [MeV]
Al 1
V 2
Yb 3
W 4
Au 5
Bi 6
1
2
3
4
5
6

Fig. 8

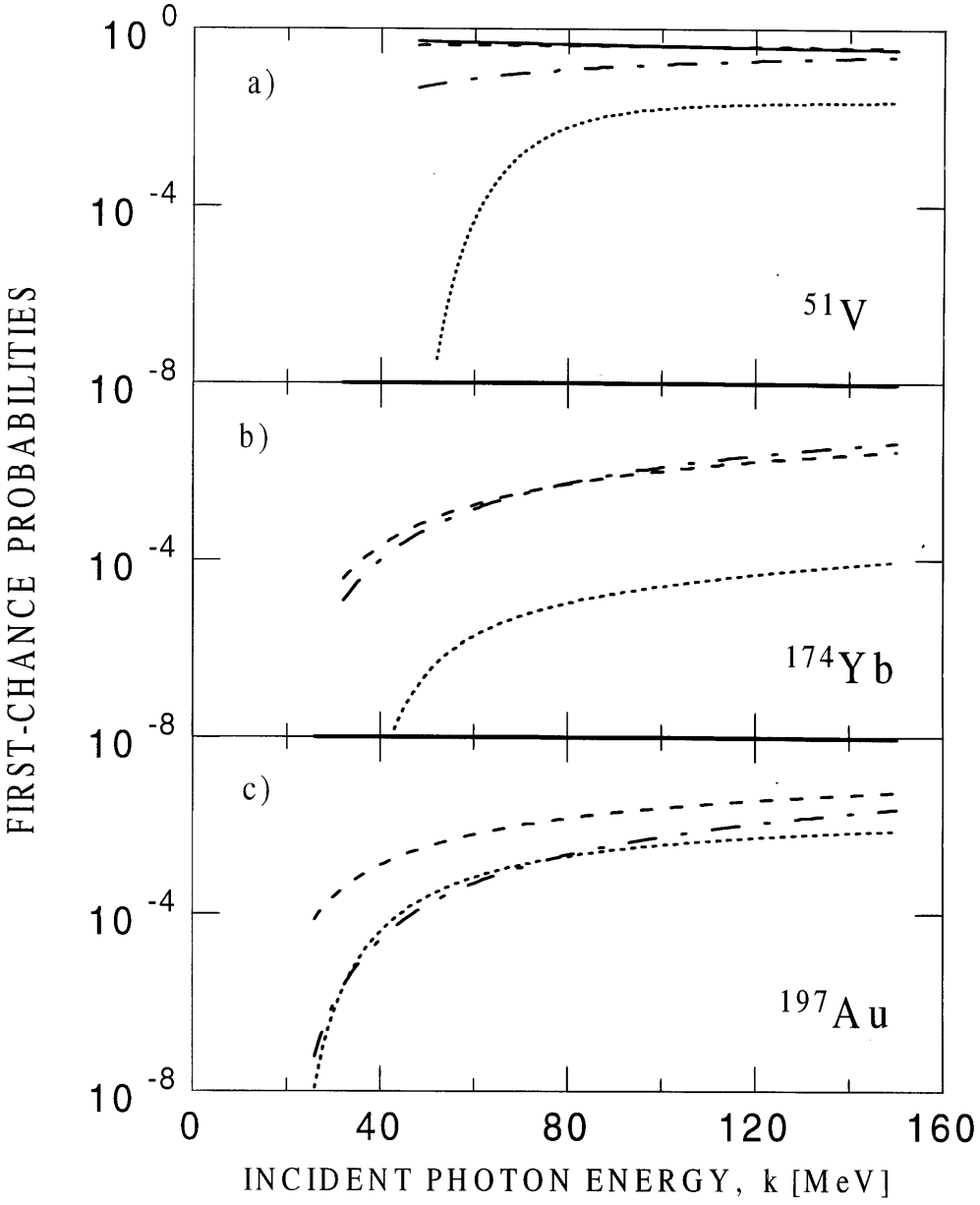
FIRST-CHANCE PROBABILITIES
10 0
10 -4
10 -8
a)
51V
b)
174Yb
c)
197Au
0
40
80
120
160
INCIDENT PHOTON ENERGY, k [MeV]

Fig. 9

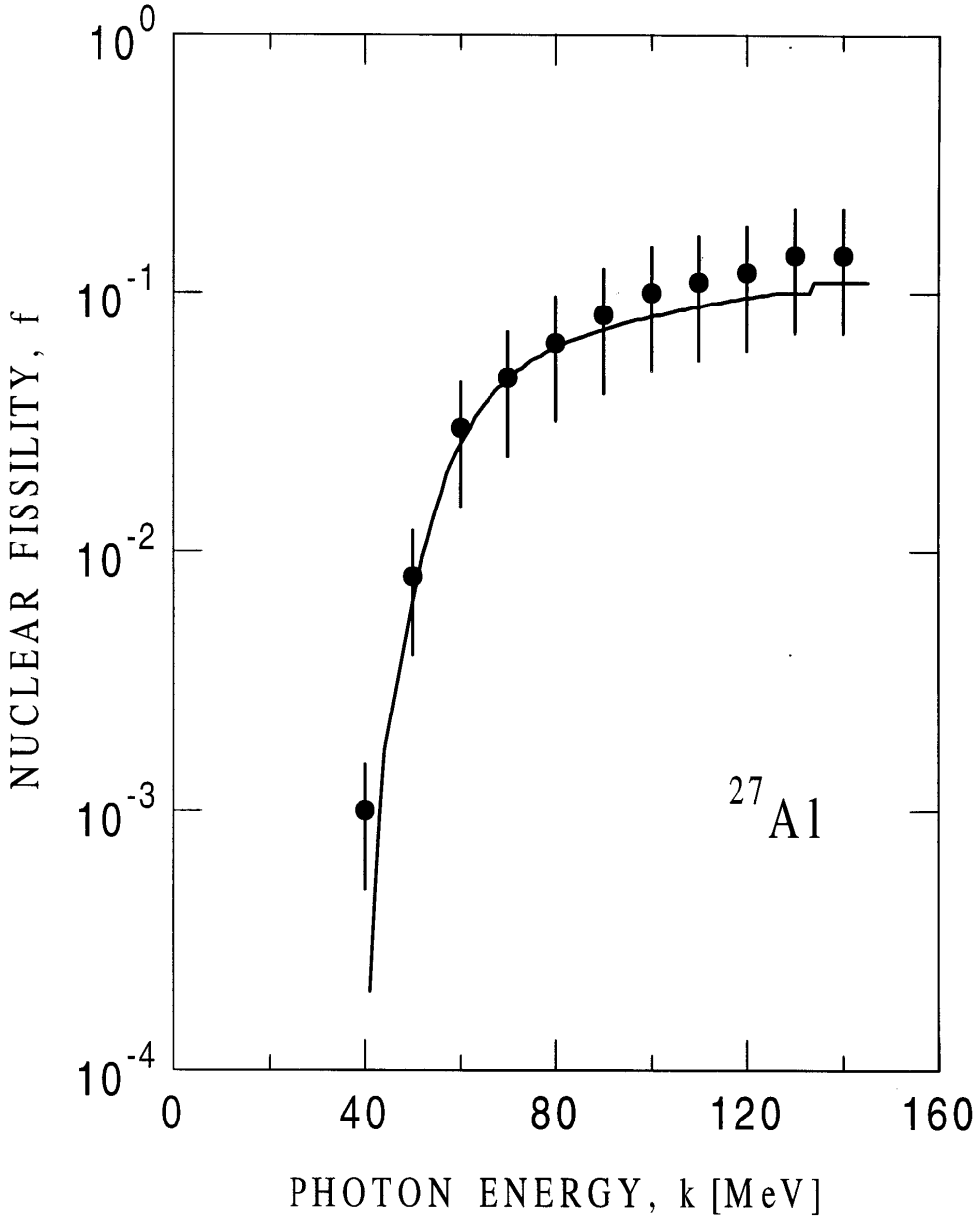
NUCLEAR FISSILITY, f
10^{0}
10^{-1}
10^{-2}
10^{-3}
10^{-4}
^{27}Al
0
40
80
120
160
PHOTON ENERGY, k [MeV]

Fig. 10

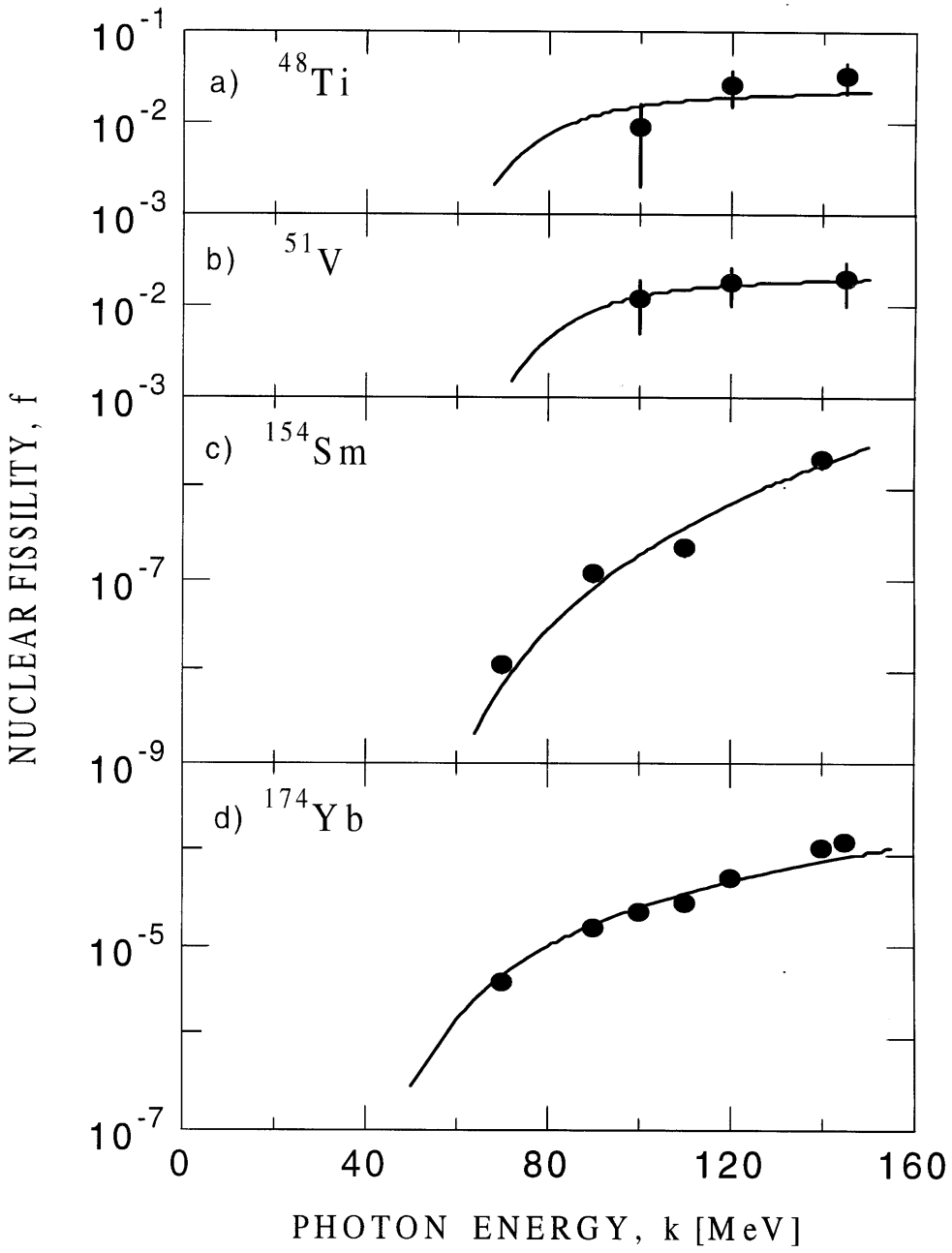
a) 48Ti
b) 51V
c) 154Sm
d) 174Yb
NUCLEAR FISSILITY, f
PHOTON ENERGY, k [MeV]
10-1
10-2
10-3
10-2
10-3
10-7
10-9
10-5
10-7
0
40
80
120
160

Fig. 11

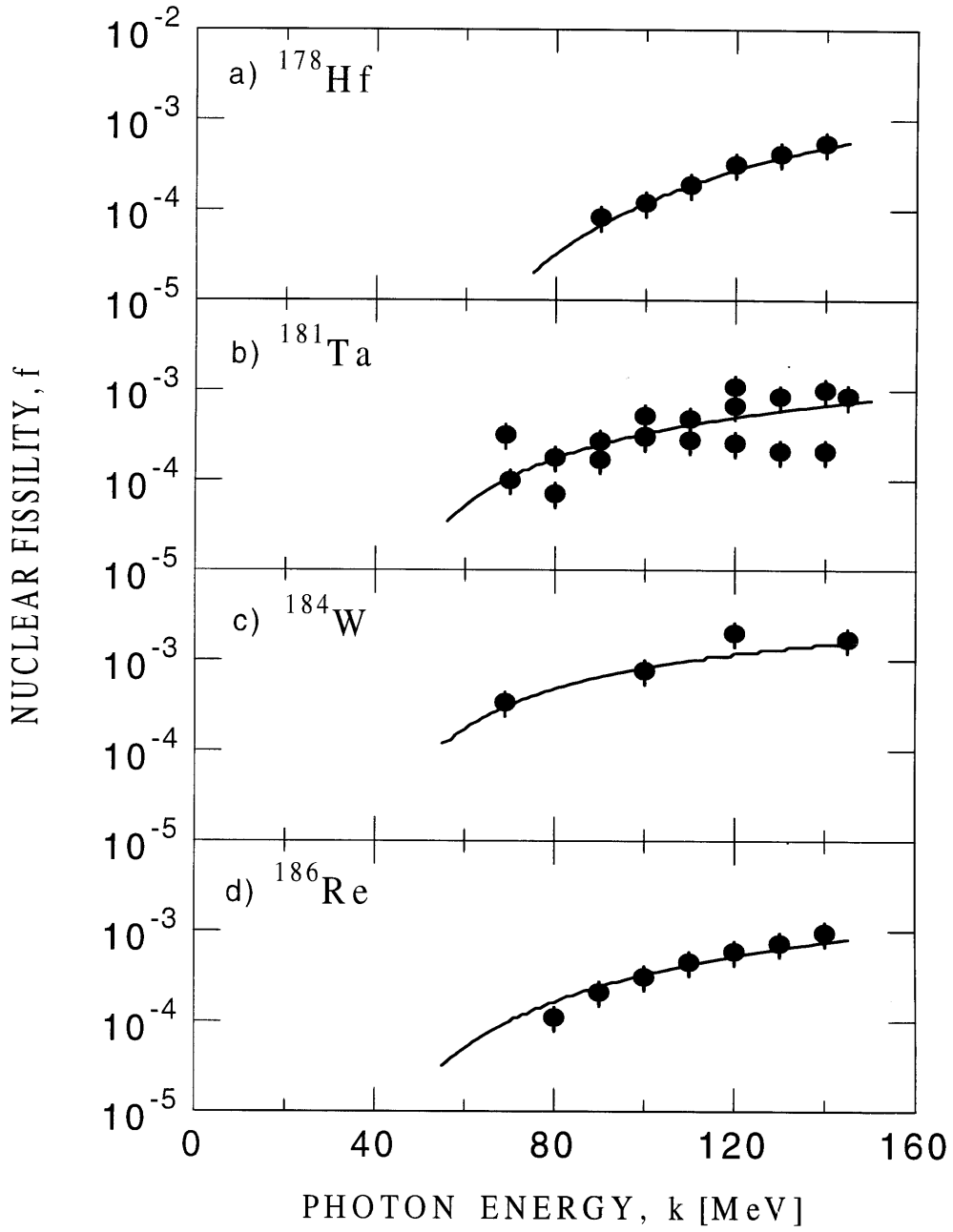
a) 178Hf
b) 181Ta
c) 184W
d) 186Re
NUCLEAR FISSILITY, f
PHOTON ENERGY, k [MeV]
10-2
10-3
10-4
10-5
0
40
80
120
160

Fig. 12

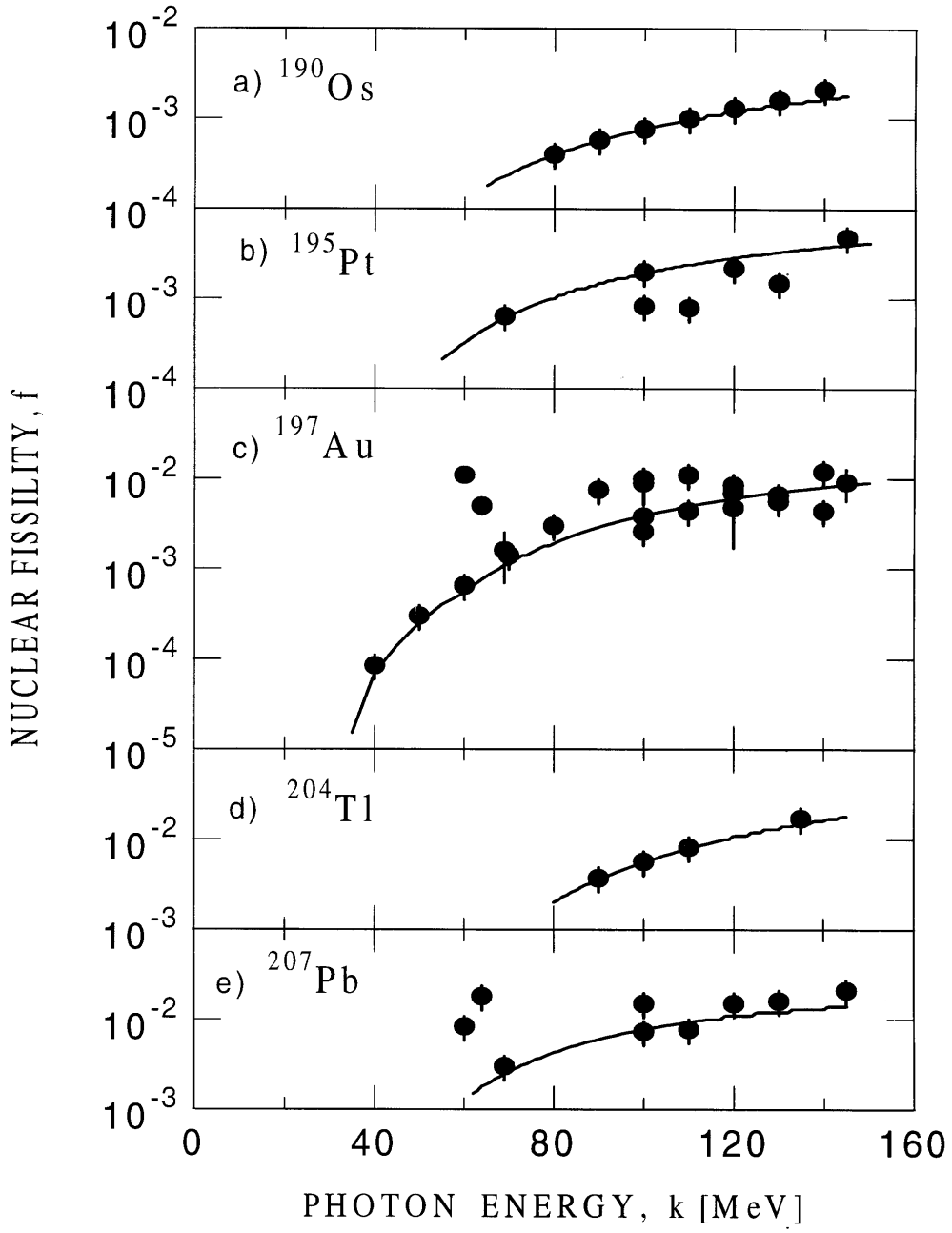
NUCLEAR FISSILITY, f
a) ^{190}Os
b) ^{195}Pt
c) ^{197}Au
d) ^{204}Tl
e) ^{207}Pb
10^{-2}
10^{-3}
10^{-4}
10^{-5}
0
40
80
120
160
PHOTON ENERGY, k [MeV]

Fig. 13

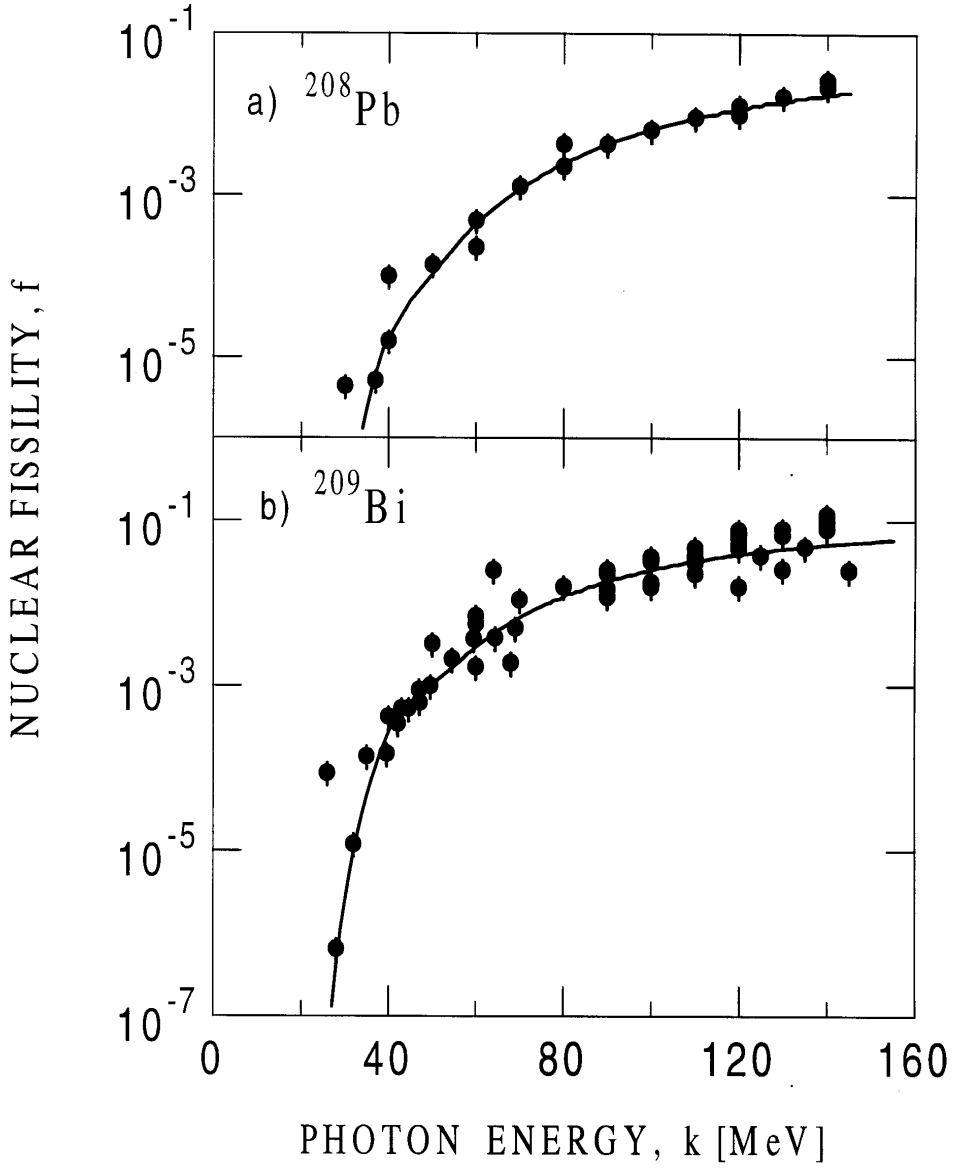
NUCLEAR FISSILITY, f
a) ^{208}Pb
b) ^{209}Bi
10^{-1}
10^{-3}
10^{-5}
10^{-7}
0
40
80
120
160
PHOTON ENERGY, k [MeV]

Fig. 14

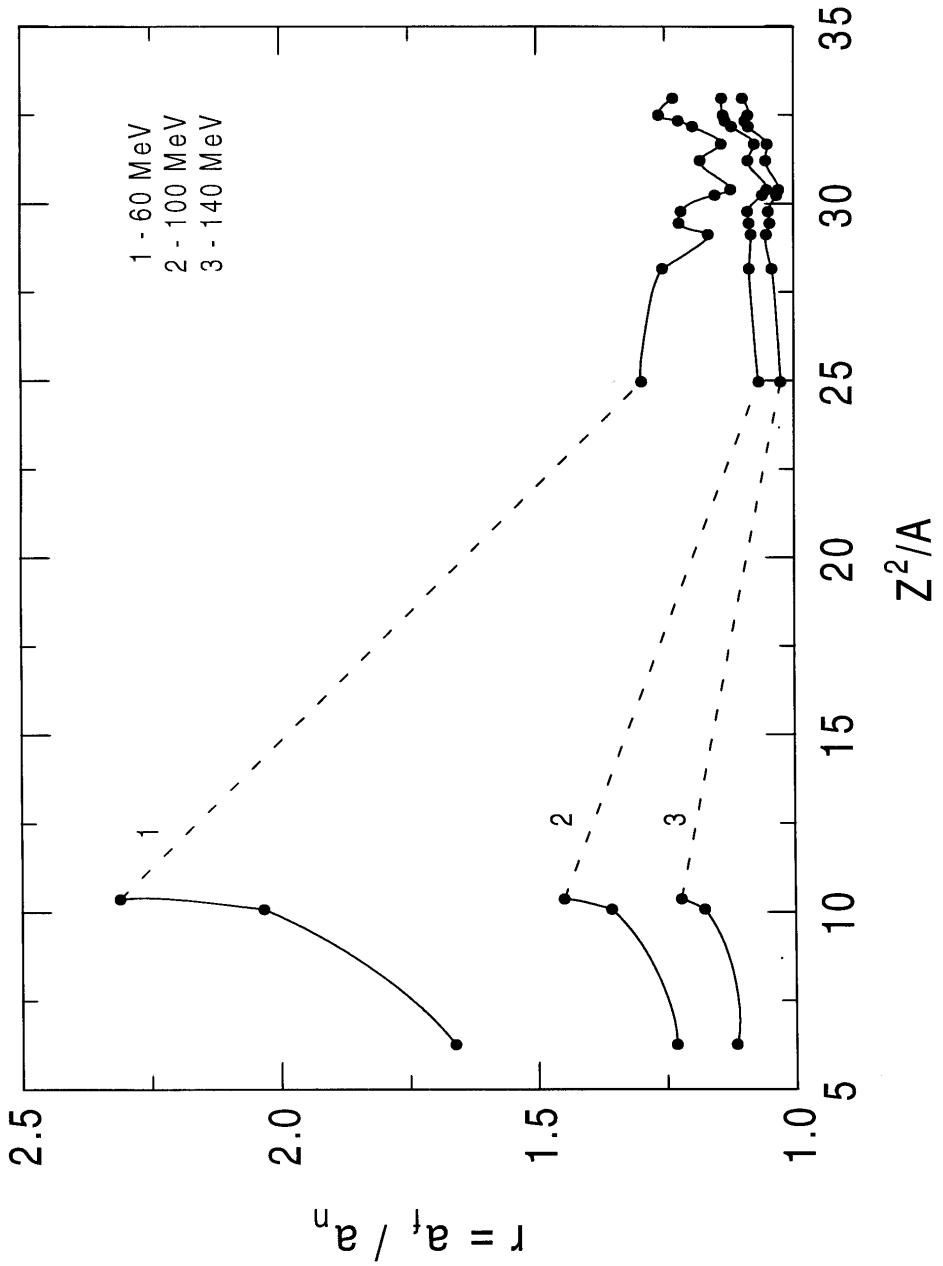
1 - 60 MeV
2 - 100 MeV
3 - 140 MeV
1
2
3
r = a_f / a_n
Z²/A
2.5
2.0
1.5
1.0
5
10
15
20
25
30
35

Fig. 15

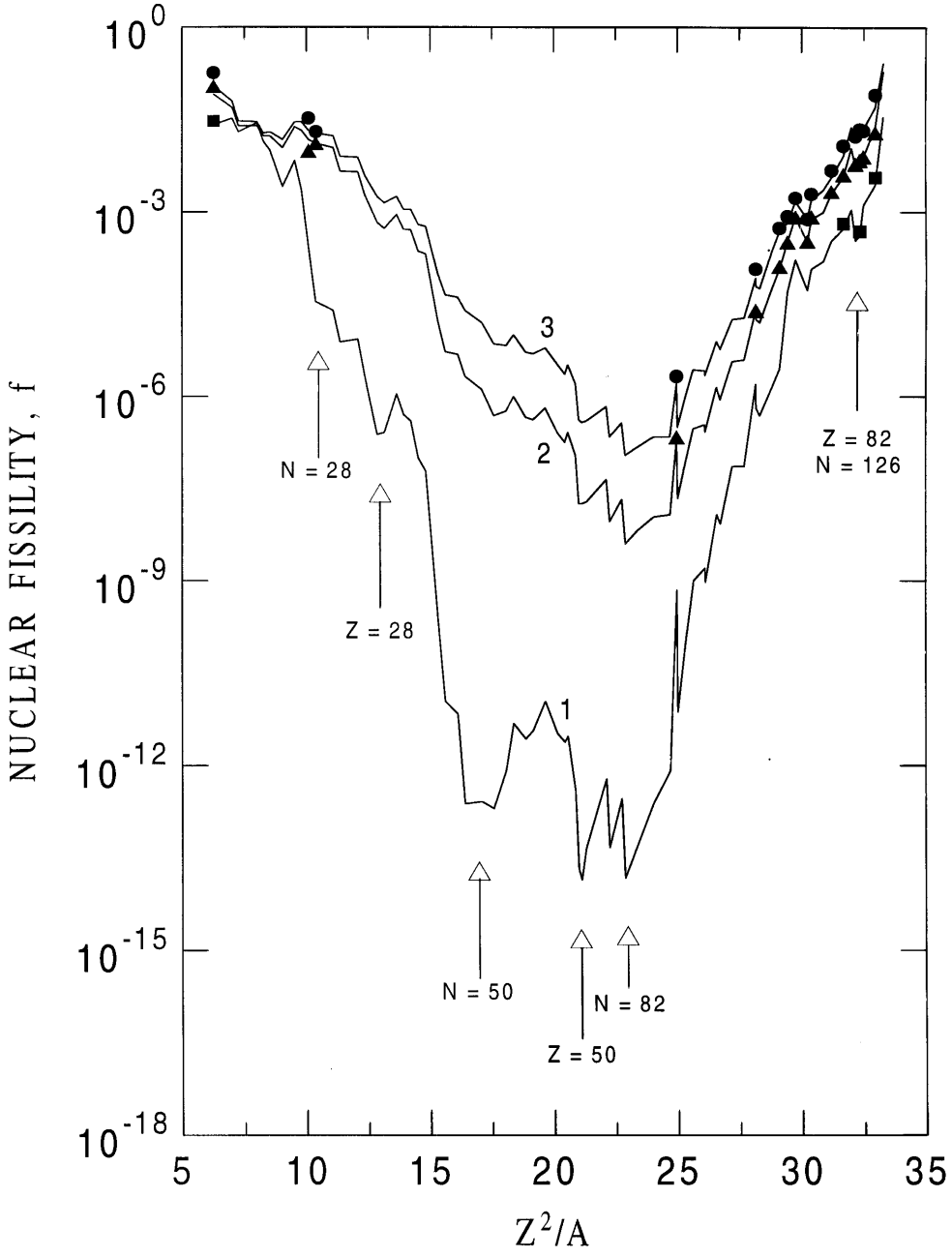
NUCLEAR FISSILITY, f
10^{0}
10^{-3}
10^{-6}
10^{-9}
10^{-12}
10^{-15}
10^{-18}
5
10
15
20
25
30
35
Z^2/A
1
2
3
N = 28
Z = 28
N = 50
Z = 50
N = 82
Z = 82
N = 126

Fig. 16

Table 1 - Values of the nuclear quantities used in the present analysis of photofissility.

Target nucleus	Nuclear radius	Fermi energy		Binding energy [c]		Coulomb energy	Cut-off energy [e]		Photon energy limiting values [f]	
		protons	neutrons	proton	neutron	at nuclear surface [d]	protons	neutrons		
	R(fm) [b]	E_F^p(MeV)	E_F^n(MeV)	B_p(MeV)	B_n(MeV)	V_p^c(MeV)	E_C^p(MeV)	E_C^n(MeV)	k_{qd}(MeV)	k_r(MeV)
^{27}Al	3.94	27.2	28.5	8.27	13.06	3.47	38.9	41.6	22.3	47
^{48}Ti [a]	4.64	27.9	31.2	11.44	11.63	5.32	44.7	42.8	23.6	52
^{51}V	4.65	28.6	32.6	8.06	11.05	5.55	42.2	43.6	24.5	49
^{154}Sm	6.60	27.4	35.7	9.09	7.97	11.50	48.0	43.7	25.2	54
^{174}Yb	6.85	27.7	36.0	7.98	7.46	12.67	48.3	43.5	25.5	54
^{178}Hf [a]	6.89	27.8	36.0	7.34	7.63	12.80	47.9	43.6	25.5	53
^{181}Ta	6.91	27.9	36.3	5.94	7.58	12.95	46.8	43.9	25.7	52
^{184}W [a]	6.92	28.1	36.5	7.70	7.41	13.14	48.9	43.9	25.8	54
^{186}Re [a]	6.95	28.1	36.5	5.83	6.18	13.26	47.2	42.7	25.8	51
^{190}Os [a]	6.98	28.1	36.9	8.02	7.79	13.46	49.6	44.7	26.0	55
^{195}Pt [a]	7.01	28.4	37.2	7.57	6.10	13.71	49.7	43.3	26.2	54
^{197}Au	7.02	28.5	37.3	5.78	8.07	13.92	48.2	45.4	26.3	54
^{204}Tl [a]	7.07	28.6	37.8	6.36	6.65	14.11	49.1	44.4	26.6	54
^{208}Pb	7.10	28.6	38.0	8.01	7.37	14.27	50.9	45.4	26.6	56
^{207}Pb [a]	7.09	28.6	37.9	7.49	6.74	14.27	50.4	44.6	26.6	55
^{209}Bi	7.13	28.6	37.7	3.80	7.46	14.39	46.8	45.2	26.5	52

[a] Mean mass number of the naturally occurring isotopes.

[b] This is given by $R = (5/3)^{1/2}\langle r^2\rangle^{1/2}$, where values of $\langle r^2\rangle^{1/2}$ are those reported in [30].

[c] Values taken from "The 1993 Atomic Mass Evaluation" by Audi and Waptra [31].

[d] Calculated by $V_p^c = 1.12(Z-1)/(\langle r^2\rangle^{1/2}_{Z-1} + 0.852)$ MeV.

[e] $E_C^p = E_F^p + B_p + V_p^c$; $E_C^n = E_F^n + B_n$.

[f] Minimum energy for quasi-deuteron photointeraction, $k_{qd} = (2/5)(E_F^n + E_F^p)$; maximum energy for simultaneous retention of neutron and proton, $k_r = (E_C^n + E_C^p) - (3/5)(E_F^n + E_F^p)$.

Table 2 – Values of the parameters α, β, γ (for neutron) and α', β', γ' (for proton) in Eq. (2).

Target nucleus	α	β (10^{-4}MeV^{-1})	γ (10^{6}MeV^{4})	α'	β' (10^{-3}MeV^{-1})	γ' (10^{6}MeV^{4})
^{27}Al	0.266	11.1	1.06	0.2308	1.26	0.882
^{48}Ti	0.242	7.75	1.42	0.1310	1.43	1.134
^{51}V	0.249	6.45	1.61	0.1337	1.24	1.189
^{154}Sm	0.184	3.71	2.12	0.0123	1.24	0.893
^{174}Yb	0.177	3.29	2.13	0.0001	1.26	0.941
^{178}Hf	0.171	3.47	2.16	0.0069	1.19	0.912
^{181}Ta	0.171	3.34	2.25	0.0036	1.20	0.922
^{184}W	0.170	3.20	2.30	-0.0024	1.24	0.954
^{186}Re	0.174	2.88	2.15	-0.0003	1.20	0.985
^{190}Os	0.172	2.90	2.39	0.0075	1.09	0.897
^{195}Pt	0.174	2.55	2.36	0.0121	1.02	0.916
^{197}Au	0.166	2.88	2.62	-0.0036	1.17	1.021
^{204}Tl	0.173	2.26	2.58	-0.0059	1.15	1.007
^{208}Pb	0.171	2.27	2.74	0.0059	1.01	0.932
^{207}Pb	0.172	2.21	2.53	-0.0020	1.09	1.012
^{209}Bi	0.169	2.40	2.64	0.0022	1.06	0.951

Table 3 – Listing of the values of parameters p and q in Eq. (30), the number of semiempirical r-values, n, and of the limiting values $k_f = (B_{f_0}^{-1} + B^{-1})^{-1}$.

Fissioning nucleus	p	q	n	k_f (MeV)
^{27}Al	2.923×10^3	2.050	10	35.5
^{48}Ti	5.250×10^3	2.084	10	44.1
^{51}V	7.085×10^3	2.099	10	47.2
^{154}Sm	3.805×10^4	2.873	4	39.9
^{174}Yb	1.511×10^3	2.122	11	31.0
^{178}Hf	4.186×10^1	1.351	6	28.2
^{181}Ta	4.456×10^2	1.857	17	26.4
^{184}W	2.951×10^2	1.761	11	24.8
^{186}Re	2.534×10^2	1.812	11	23.1
^{190}Os	1.176×10^2	1.679	11	22.5
^{195}Pt	6.032×10^1	1.419	12	21.8
^{197}Au	1.840×10^1	1.191	17	21.5
^{204}Tl	0.947×10^1	0.948	11	22.7
^{208}Pb	1.446×10^1	1.019	17	24.0
^{207}Pb	5.096×10^1	1.287	11	23.3
^{209}Bi	1.502×10^1	1.016	54	22.1

Figure Captions

Fig. 1 – Variation of laboratory neutron and proton kinetic energies in the final state (T_{n^*} and T_{p^*}, respectively) with proton angle in the center-of-mass system, θ'_p, for a 100-MeV primary quasi-deuteron photointeraction in ^{184}W target nucleus. The range of θ'_p within which the interaction is allowed according to the Pauli exclusion principle is indicated. Note that whatever θ'_p, $T_{n^*} + T_{p^*} = k + (3/5)(E_F^n + E_F^p) \approx 139$ MeV.

Fig. 2 – Nuclear transparency for ^{27}Al, ^{154}Sm, and ^{209}Bi target nuclei to emergent neutron, τ_{n^*}, and proton, τ_{p^*}, plotted against particle kinetic energy, T_{n^*} or T_{p^*}, inside the nucleus.

Fig. 3 – Average probability of formation of residual nuclei $\overline{p}_i (i = 0, 1, 2, 3)$ plotted against mass number A of the target nucleus. The modes of formation of residuals from the interaction $\gamma + (\mathrm{n} + \mathrm{p}) \rightarrow \mathrm{n}^* + \mathrm{p}^*$ are: simultaneous escaping of neutron and proton ($i = 0$), escaping of neutron alone ($i = 1$), escaping of proton alone ($i = 2$), and simultaneous retention of neutron and proton ($i = 3$). It is shown the cases for 100-MeV incident photon.

Fig. 4 – Part a) shows the quantity $\overline{p}_i$ (as defined in Fig. 3), and part b) shows the corresponding average excitation energy of residuals, $\overline{E_i^*} (i = 0, 1, 2, 3)$ as a function of incident photon energy for ^{145}Sm target nucleus.

Fig. 5 – The quantity $\overline{p}_3$ (as defined in Fig. 3) plotted against incident photon energy for various target nuclei as indicated.

Fig. 6 – Schematic representation of the fission-evaporation competition process for an excited, residual nucleus (Z, A, E^*). The meaning of the symbols is explained in the text (section 2.4).

Fig. 7 – Level-density parameter after neutron evaporation, a_n, plotted against excitation energy for various nuclei according to the parametrization by Iljinov et al. [40].

Results are given for ^{51}V, ^{48}Ti, and ^{27}Al (part a) and for other pre-actinide nuclei as indicated (part b).

Fig. 8 – Variation of the ratio $r = a_f/a_n$ with excitation energy of the fissioning nucleus. The curves are least-squares fitting of the semi-empirical r-values obtained as explained in the text (see also Table 3). Results are given for six representative nuclei as indicated.

Fig. 9 – Absolute first-chance probabilities for neutron emission (P_{n_1}, full line), proton emission (P_{p_1}, dashed line), alpha-particle emission (P_{α_1}, dash-dotted line), and fission (f_1, dotted line) plotted against photon energy. Results are shown for three representative residual (or target) nuclei: ^{51}V (a), ^{174}Yb (b), and ^{197}Au (c). The curves are calculated trends as explained in the text (section 2.5).

Fig. 10 – Nuclear fissility plotted against incident photon energy for ^{27}Al target nucleus. The full line represents the calculated trend according to Eqs. (31) and (32) in the text. Experimental data (points) are taken at 10-MeV intervals from the fissility curve reported in [13].

Fig. 11 – The same as in Fig. 10 for ^{48}Ti (part a), ^{51}V (part b), ^{154}Sm (part c), and ^{174}Yb (part d). Experimental data (points) are taken from Refs. [10,12] for Ti and V targets, and from Ref. [20] for Sm and Yb targets.

Fig.12 – The same as in Fig. 10 for ^{178}Hf (part a), ^{181}Ta (part b), ^{184}W (part c), and ^{186}Re (part d). Experimental data (points) are taken from Refs. [9,10,12,23] for Ta, from Refs. [9,10,12] for W, and from extrapolated, measured photofission cross section curves for Hf, Ta, and Re targets as reported in [17].

Fig. 13 – The same as in Fig. 10 for ^{190}Os (part a), ^{195}Pt (part b), ^{197}Au (part c), ^{204}Tl (part d), and ^{207}Pb (part e). Experimental data (points) are taken from an extrapolated, measured photofission cross section curve for Os as reported in [17], from Refs. [9,10,12,17,18] for Pt, from Refs. [5,7,10,12,17,18,23] for Au, from Refs. [16,18] for Tl, and from Refs. [5,7,10,12,17,18] ^{207}Pb.

Fig. 14 – The same as in Fig. 10 for ^{208}Pb and ^{209}Bi. Experimental data are taken from Refs. [2-5,7,10-12,14-17,19-21] for Bi target, and from Refs. [20,22] for ^{208}Pb target.

Fig. 15 – The ratio $r = a_f/a_n$ is plotted against parameter Z^2/A of the fissioning system (target nucleus). The smoothed lines connect semiempirical determination of r-values (points) at 60-, 100-, and 140-MeV incident photon energies ($k = E^*$) as calculated by eq. (30). The dashed portions of the lines show the region of nuclei ($\sim$ Mn-La) where r-values are not yet defined from photofission experiments.

Fig. 16 – Nuclear fissility *versus* parameter Z^2/A for 60-MeV (curve 1), 100-MeV (curve 2), and 140-MeV (curve 3) incident photon energy (excitation energy). At each energy, the broken line connects calculated f-values for nuclei ranging from aluminium to polonium along the beta-stability valley; structures due mainly to pairing and/or shell effects are clearly seen. Some experimental points are shown to allow a comparison: ■, at 60 MeV from Refs. [2,13,22,23]; ▲, at 100 MeV from Refs. [10,13,17,18,20,22,23]; and •, at 140 MeV from Refs. [6,12,13,15-17,20,22].The same as in Fig. 10 for ^{209}Bi. Experimental data are taken from Refs. [2-5,7,10-12,14-17,19-21].